

Ground-state properties of the symmetric single-impurity Anderson model on a ring from Density-Matrix Renormalization Group, Hartree-Fock, and Gutzwiller theory

Gergely Barcza¹, Florian Gebhard^{2,*}, Thorben Linneweber², and Örs Legeza¹

¹*Strongly Correlated Systems Lendület Research Group, Institute for Solid State Physics and Optics, MTA Wigner Research Centre for Physics, P.O. Box 49, H-1525 Budapest, Hungary and*
²*Fachbereich Physik, Philipps-Universität Marburg, D-35032 Marburg, Germany*

(Dated: June 5, 2018)

We analyze the ground-state energy, magnetization, magnetic susceptibility, and Kondo screening cloud of the symmetric single-impurity Anderson model (SIAM) that is characterized by the band width W , the impurity interaction strength U , and the local hybridization V . We compare Gutzwiller variational and magnetic Hartree-Fock results in the thermodynamic limit with numerically exact data from the Density-Matrix Renormalization Group (DMRG) method on large rings. To improve the DMRG performance, we use a canonical transformation to map the SIAM onto a chain with half the system size and open boundary conditions. We compare to Bethe-Ansatz results for the ground-state energy, magnetization, and spin susceptibility that become exact in the wide-band limit. Our detailed comparison shows that the field-theoretical description is applicable to the SIAM on a ring for a broad parameter range. Hartree-Fock theory gives an excellent ground-state energy and local moment for intermediate and strong interactions. However, it lacks spin fluctuations and thus cannot screen the impurity spin. The Gutzwiller variational energy bound becomes very poor for large interactions because it does not describe properly the charge fluctuations. Nevertheless, the Gutzwiller approach provides a qualitatively correct description of the zero-field susceptibility and the Kondo screening cloud. The DMRG provides excellent data for the ground-state energy and the magnetization for finite external fields. At strong interactions, finite-size effects make it extremely difficult to recover the exponentially large zero-field susceptibility and the mesoscopically large Kondo screening cloud.

PACS numbers: 72.15.Qm, 75.20.Hr, 75.30.Hx

I. INTRODUCTION

The single-impurity Anderson model (SIAM) describes an impurity where electrons interact locally in a metallic host.^{1,2} It poses one of the best studied and understood fundamental many-body problems; for a review, see Ref. [3]. Therefore, it still serves as a benchmark test for the development of advanced analytical many-body techniques, e.g., the functional renormalization group technique.^{4–6} For the symmetric SIAM, the low-energy physics is similar to that of the single-impurity *s-d* or Kondo model^{7,8} where an impurity spin couples to the host electrons' spin degrees of freedom: at zero temperature, the impurity local moment is screened by the host electrons which gives rise to a narrow Abrikosov-Suhl or Kondo resonance in the impurity spectral function at the Fermi level.³ The resonance can be resolved using the Numerical Renormalization Group (NRG) technique; for a review, see Ref. [9]. At higher energies, Hubbard satellites appear in the impurity spectral function that describe the local charge fluctuations. Both the Kondo resonance and the Hubbard satellite are accessible from the analytic Local-Moment Approach.^{10–12}

More recently, the real-space features of the screening were studied for the Kondo model using NRG,^{13–15} and the analytical coherent-state expansion.¹⁶ For the non-interacting SIAM (resonant-level model) in the wide-band limit, the screening cloud was analyzed analytically,¹⁷ and the magnetic properties of the interacting SIAM were studied numerically using the Density Matrix

Renormalization Group (DMRG) method.¹⁸ The various methods show that the screening cloud extends very far into the host metal. In the Kondo regime, an algebraic decay sets in only beyond a characteristic (Kondo) length scale that is proportional to the inverse of the Kondo temperature.

Less attention was dedicated to ground-state properties of the SIAM and Kondo models because they are solvable by Bethe Ansatz.^{19–22} Therefore, important quantities such as the ground-state energy, magnetization, and magnetic susceptibility at zero field are known explicitly. The Bethe Ansatz is based on the wide-band limit, $W \rightarrow \infty$, so that the dispersion relation of the host electrons can be linearized around the Fermi energy. However, the implicit assumption that the Hubbard interaction U is small compared to the bandwidth, $U \ll W$, impedes a comparison with methods that treat the SIAM on a lattice such as the DMRG method, and the Hartree-Fock¹ and Gutzwiller wave functions.^{23,24}

In this work, we use the DMRG to calculate numerically exactly the ground-state energy, the local magnetic moment, the zero-field susceptibility, and the screening cloud of the single-impurity Anderson model on large rings. The Gutzwiller and Hartree-Fock approaches provide complementary insights. The Hartree-Fock variational estimate of the ground-state energy is very satisfactory for moderate to large Hubbard interactions whereas the Gutzwiller estimate is acceptable only for small U . On the other hand, the Gutzwiller approach provides a qualitatively correct description of the magnetic proper-

ties whereas Hartree-Fock theory fails to screen the impurity spin even at infinitely large distances. Since the Gutzwiller approach is heavily based on the exact results for the non-interacting SIAM, we compile the results for the resonant-level model in the supplemental material.²⁵

Our work is structured as follows. In Sect. II, we introduce the one-dimensional SIAM on a ring with local hybridization at particle-hole and spin symmetry. We map the model onto a two-chain problem^{26,27} where the two chains separate in the thermodynamic limit. The reduced model provides the basis for our numerical DMRG investigations. In Sect. III we discuss the ground-state energy, magnetization, and spin correlation function between the impurity and the bath sites for the non-interacting SIAM for small hybridizations. The derivation of the formulae is deferred to the supplemental material. In Sect. IV, we evaluate the Gutzwiller variational wave function for the SIAM and determine an analytical variational upper bound for the ground-state energy. Moreover, we calculate the variational magnetization and spin correlation function. In Sect. V we compare our results for the ground-state energy, magnetization, and the spin correlation function with numerically exact DMRG data for large system sizes. We include the results from Bethe Ansatz and a magnetic Hartree-Fock calculation, see the supplemental material for their derivation.²⁵ Short conclusions, Sect. VI, close our presentation.

II. SYMMETRIC SINGLE-IMPURITY ANDERSON MODEL ON A RING

We study the particle-hole and spin symmetric SIAM on a ring.^{1,2} For strong interactions, this model maps onto the one-dimensional Kondo impurity model.²⁸

A. Hamiltonian

The Hamilton operator for the one-dimensional single-impurity Anderson model reads^{1,3}

$$\begin{aligned}\hat{H} &= \hat{H}_0 + \hat{H}_{\text{int}} , \\ \hat{H}_{\text{int}} &= U (\hat{n}_{d,\uparrow} - 1/2) (\hat{n}_{d,\downarrow} - 1/2) ,\end{aligned}\quad (1)$$

where $\hat{n}_{d,\sigma} = \hat{d}_{\sigma}^+ \hat{d}_{\sigma}$ counts the number of σ -electrons on the impurity site ($\sigma = \uparrow, \downarrow$). Only the electrons on the impurity site repel each other with strengths $U > 0$. The non-interacting Hamiltonian,

$$\hat{H}_0 = \hat{T} + \hat{B} + \hat{V} + \hat{P} , \quad (2)$$

describes bath electrons that move between neighboring sites on a ring with L sites,

$$\hat{T} = -\frac{W}{4} \sum_{n=0,\sigma}^{L-1} (\hat{c}_{n,\sigma}^+ \hat{c}_{n+1,\sigma} + \hat{c}_{n+1,\sigma}^+ \hat{c}_{n,\sigma}) , \quad (3)$$

where the band width provides our unit of energy, $W \equiv 1$.

In the presence of an external magnetic field $\mathcal{H}_{\text{bath}}$ we may include the magnetic term

$$\hat{B} = -B_{\text{bath}} \sum_{n=0}^{L-1} (\hat{c}_{n,\uparrow}^+ \hat{c}_{n,\uparrow} - \hat{c}_{n,\downarrow}^+ \hat{c}_{n,\downarrow}) . \quad (4)$$

Here, we abbreviated $B_{\text{bath}} = g\mu_{\text{B}}\mathcal{H}_{\text{bath}}/2$ where μ_{B} is the Bohr magneton and $g \approx 2$ is the electrons' gyromagnetic factor.

The bath electrons hybridize at the origin, $n = 0$, with the impurity electrons with strength $V > 0$,

$$\hat{V} = V \sum_{\sigma} (\hat{d}_{\sigma}^+ \hat{c}_{0,\sigma} + \hat{c}_{0,\sigma}^+ \hat{d}_{\sigma}) . \quad (5)$$

The system is half filled, i.e., the total number of electrons is $N = L + 1$, and we investigate a paramagnetic situation, $N_{\uparrow} = N_{\downarrow} = (L+1)/2$. Consequently, the number of bath sites L must be odd. From now on we further assume that $(L+3)/2$ is even.

There can be a local, possibly spin-dependent potential,

$$\hat{P} = - \sum_{\sigma} E_{d,\sigma} \left(\hat{n}_{d,\sigma} - \frac{1}{2} \right) . \quad (6)$$

In the presence of an external magnetic field \mathcal{H}_{imp} at the impurity we have $E_{d,\uparrow} = (g\mu_{\text{B}}/2)\mathcal{H}_{\text{imp}} = -E_{d,\downarrow}$. In the magnetic Hartree-Fock approach, we have $E_{d,\uparrow} = Um = -E_{d,\downarrow}$ where the value of the \hat{S}_z at the impurity, $m = \langle \hat{n}_{d,\uparrow} - \hat{n}_{d,\downarrow} \rangle / 2$, has to be determined self-consistently.²⁵

B. Particle-hole symmetry

To analyze particle-hole symmetry in the SIAM, we set $E_{d,\sigma} = 0$ and $\mathcal{H}_{\text{bath}} = 0$ in the rest of this section, i.e., we have no magnetic symmetry breaking. Particle-hole symmetry for the SIAM was studied previously, e.g., in Ref. [29].

1. Wave numbers and particle-hole boundary conditions

For a ring, the kinetic energy is diagonal in momentum space,

$$\hat{T} = \sum_{k,\sigma} \epsilon(k) \hat{c}_{k,\sigma}^+ \hat{c}_{k,\sigma} , \quad (7)$$

where

$$\hat{c}_{n,\sigma} = \sqrt{\frac{1}{L}} \sum_k e^{ikn} \hat{c}_{k,\sigma} \quad , \quad \hat{c}_{k,\sigma} = \sqrt{\frac{1}{L}} \sum_{n=0}^{L-1} e^{-ikn} \hat{c}_{n,\sigma} , \quad (8)$$

and the dispersion relation is given by

$$\epsilon(k) = -\cos(k)/2 . \quad (9)$$

In one dimension $Q = \pi$ is half a reciprocal lattice vector, $\epsilon(k + 2Q) = \epsilon(k)$. For particle-hole symmetry we must demand that

$$\epsilon(\pi - k) = -\epsilon(k) \quad (10)$$

for all accessible $|k| \leq \pi$. In particular, this equation implies that with k , also $\pi - k$ is an accessible k -value. This is not difficult to fulfill for even L but poses a problem for odd L .

Let

$$k_m = \frac{2\pi}{L}m + \varphi, \quad m = -(L-1)/2, \dots, (L-1)/2, \quad (11)$$

where $0 \leq \varphi < 2\pi/L$ and k_m are defined modulo 2π . Then, the set of k -values must also be given by

$$\begin{aligned} k'_m &= \pi - \frac{2\pi}{L}m - \varphi = \frac{2\pi}{L} \left(\frac{L-1}{2} + \frac{1}{2} - m \right) + \varphi - 2\varphi \\ &= \frac{2\pi}{L} \left(\frac{L-1}{2} - m \right) + \varphi + \frac{\pi - 2\varphi L}{L}. \end{aligned} \quad (12)$$

Using the definition of the accessible k -values, we see that we must set

$$\varphi = \pm\pi/(2L) \quad (13)$$

to make the sets $\{k\}$ and $\{k'\}$ identical.

The accessible k -values belong to the boundary conditions

$$e^{ik_m L} = e^{i\pi/2} = i, \quad (14)$$

i.e., they are neither periodic nor anti-periodic. We call these boundary conditions *particle-hole periodic*. They imply $\hat{c}_L = i\hat{c}_0$ ($\hat{c}_L^+ = -i\hat{c}_0^+$) in position space so that we may write for the kinetic energy in eq. (2)

$$\begin{aligned} \hat{T} &= -\frac{1}{4} \sum_{n=0,\sigma}^{L-2} (\hat{c}_{n,\sigma}^+ \hat{c}_{n+1,\sigma} + \hat{c}_{n+1,\sigma}^+ \hat{c}_{n,\sigma}) \\ &\quad -\frac{1}{4} \left(i\hat{c}_{L-1,\sigma}^+ \hat{c}_{0,\sigma} - i\hat{c}_{0,\sigma}^+ \hat{c}_{L-1,\sigma} \right). \end{aligned} \quad (15)$$

Eq. (15) shows that the kinetic energy is indeed invariant under the particle-hole transformation

$$\text{ph: } \hat{c}_{n,\sigma} \mapsto (-1)^n \hat{c}_{n,\sigma}^+ \quad \text{for } n = 0, 1, \dots, L-1 \quad (16)$$

because either n or $n+1$ is even when the other is odd, and the origin and $L-1$ are both even numbers for odd L .

2. Model properties at particle-hole symmetry

For the one-dimensional model (2) with particle-hole boundary conditions and $E_{d,\sigma} = 0$, we define the particle-hole transformation

$$\begin{aligned} \text{ph: } \hat{c}_{n,\sigma} &\mapsto (-1)^n \hat{c}_{n,\sigma}^+ \quad \text{for } n = 0, 1, \dots, L-1, \\ \hat{d}_\sigma &\mapsto (-1) \hat{d}_\sigma^+. \end{aligned} \quad (17)$$

It is readily seen that the transformation leaves the Hamiltonian \hat{H} invariant. The particle-number operators transform according to

$$\hat{n}_{d,\sigma} \mapsto 1 - \hat{n}_{d,\sigma}, \quad \hat{c}_{n,\sigma}^+ \hat{c}_{n,\sigma} \mapsto 1 - \hat{c}_{n,\sigma}^+ \hat{c}_{n,\sigma}, \quad (18)$$

so that the N -particle sector maps onto the sector with $2(L+1)-N$ particles. At half band-filling, $N = L+1$, the normalized ground state maps onto itself, $|\Psi_0\rangle \mapsto |\Psi_0\rangle$, up to a global phase. Therefore, particle-hole symmetry guarantees

$$\langle \Psi_0 | \hat{n}_{d,\sigma} | \Psi_0 \rangle = 1/2 \quad (19)$$

for all interaction strengths U and hybridizations V . Moreover, we obtain

$$\begin{aligned} \langle \Psi_0 | \hat{c}_{n,\sigma}^+ \hat{d}_\sigma | \Psi_0 \rangle &= (-1)^n \langle \Psi_0 | \hat{d}_\sigma^+ \hat{c}_{n,\sigma} | \Psi_0 \rangle \\ &= (-1)^n \langle \Psi_0 | \hat{c}_{n,\sigma}^+ \hat{d}_\sigma | \Psi_0 \rangle^* \end{aligned} \quad (20)$$

for the hybridization matrix element between impurity and bath electrons at site n . Therefore, the matrix elements are alternately real or purely imaginary. In momentum space, eq. (20) reads

$$M(k) \equiv \langle \Psi_0 | \hat{c}_{k,\sigma}^+ \hat{d}_\sigma | \Psi_0 \rangle = \langle \Psi_0 | \hat{c}_{\pi-k,\sigma}^+ \hat{d}_\sigma | \Psi_0 \rangle^*. \quad (21)$$

Since the wave numbers k enter the single-impurity Anderson model only via the dispersion relation, $M(k) \equiv M(\epsilon(k))$, eq. (21) implies

$$\text{Re}M(-\epsilon) = \text{Re}M(\epsilon), \quad \text{Im}M(-\epsilon) = -\text{Im}M(\epsilon) \quad (22)$$

because $\epsilon(\pi - k) = -\epsilon(k)$. We shall use this relation in Sect. III.

3. Phase shifts and periodic boundary conditions

Instead of using particle-hole periodic boundary conditions, we may distribute the phase shift $\pm\pi/2$ evenly and use periodic boundary conditions. We rewrite

$$\hat{c}_{n,\sigma} = \exp(i\varphi n) \hat{b}_{n,\sigma} \quad (23)$$

for $n = 0, 1, \dots, L-1$. Then,

$$\hat{T} = -\frac{1}{4} \sum_{n=0,\sigma}^{L-1} \left(e^{i\varphi} \hat{b}_{n,\sigma}^+ \hat{b}_{n+1,\sigma} + e^{-i\varphi} \hat{b}_{n+1,\sigma}^+ \hat{b}_{n,\sigma} \right), \quad (24)$$

where $\hat{b}_{L,\sigma} = \hat{b}_{0,\sigma}$, i.e., the b -electrons obey periodic boundary conditions.

When we Fourier transform into momentum space, we use the wave numbers

$$\tilde{k}_m = \frac{2\pi}{L}m, \quad m = 0, 1, \dots, L-1. \quad (25)$$

The kinetic energy becomes

$$\hat{T} = \sum_{\tilde{k},\sigma} (-2t \cos(\tilde{k} + \varphi)) \hat{b}_{\tilde{k},\sigma}^+ \hat{b}_{\tilde{k},\sigma}. \quad (26)$$

Therefore, the dispersion relation and the set of accessible k -values are still given by eqs. (9) and (11).

The kinetic energy operator (24) is particle-hole symmetric under the transformation

$$\text{ph} : \hat{b}_{n,\sigma} \mapsto (-1)^n e^{-2i\varphi n} \hat{b}_{n,\sigma}^+ \quad \text{for } n = 0, 1, \dots, L-1. \quad (27)$$

This is readily seen for all electron transfers between sites n and $(n+1)$ for $n = 0, 1, \dots, (L-2)$, where the value of φ is actually irrelevant. For the electron transfer between the last and first site, however, we find

$$\begin{aligned} e^{i\varphi} \hat{b}_{L-1,\sigma}^+ \hat{b}_{0,\sigma} + e^{-i\varphi} \hat{b}_{0,\sigma}^+ \hat{b}_{L-1,\sigma} &\mapsto \\ e^{i\varphi} e^{2i\varphi(L-1)} \hat{b}_{L-1,\sigma}^+ \hat{b}_{0,\sigma} + e^{-i\varphi} \hat{b}_{0,\sigma} e^{-2i\varphi(L-1)} \hat{b}_{L-1,\sigma}^+ \end{aligned} \quad (28)$$

because both the origin and the last site are even. For the transformed term to become equivalent to the original term, we must impose

$$e^{2i\varphi L} = -1 \quad (29)$$

which again gives $\varphi = \pm\pi/(2L)$ as in eq. (13).

C. Mapping onto a two-chain problem

1. Canonical transformation

For $n = 1, 2, \dots, (L-1)/2$ we perform the canonical transformation^{26,27}

$$\begin{aligned} \hat{C}_{n,\sigma} &= \sqrt{\frac{1}{2}} \left(e^{i\varphi} \hat{b}_{n,\sigma} + e^{-i\varphi} \hat{b}_{L-n,\sigma} \right), \\ \hat{S}_{n,\sigma} &= \sqrt{\frac{1}{2}} \left(e^{i\varphi} \hat{b}_{n,\sigma} - e^{-i\varphi} \hat{b}_{L-n,\sigma} \right) \end{aligned} \quad (30)$$

with the inverse transformation

$$\begin{aligned} \hat{b}_{n,\sigma} &= \sqrt{\frac{1}{2}} e^{-i\varphi} \left(\hat{C}_{n,\sigma} + \hat{S}_{n,\sigma} \right), \\ \hat{b}_{L-n,\sigma} &= \sqrt{\frac{1}{2}} e^{i\varphi} \left(\hat{C}_{n,\sigma} - \hat{S}_{n,\sigma} \right). \end{aligned} \quad (31)$$

The kinetic energy becomes

$$\begin{aligned} -4\hat{T} &= \sum_{\sigma} \left(\hat{B}_{1,\sigma} + \hat{B}_{2,\sigma} \right) \\ &+ \sum_{n=1,\sigma}^{(L-3)/2} \left(\hat{C}_{n,\sigma}^+ \hat{C}_{n+1,\sigma} + \hat{C}_{n+1,\sigma}^+ \hat{C}_{n,\sigma} \right) \\ &+ \sum_{n=1,\sigma}^{(L-3)/2} \left(\hat{S}_{n,\sigma}^+ \hat{S}_{n+1,\sigma} + \hat{S}_{n+1,\sigma}^+ \hat{S}_{n,\sigma} \right), \end{aligned} \quad (32)$$

where the boundary term at the left chain end reads

$$\hat{B}_{1,\sigma} = \sqrt{2} \left(\hat{c}_{0,\sigma}^+ \hat{C}_{1,\sigma} + \hat{C}_{1,\sigma}^+ \hat{c}_{0,\sigma} \right). \quad (33)$$

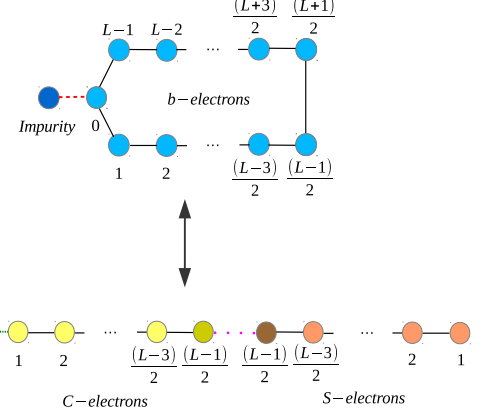


FIG. 1. (Color online) SIAM in ring geometry, eq. (1), with the kinetic energy from eq. (24), and in two-chain geometry with the kinetic energy from eq. (32). Sites with the same color have the same on-site energy, bonds with the same color have the same electron transfer amplitudes. The dotted bond between the C -electron and S -electron chains vanishes in the thermodynamic limit, $L \rightarrow \infty$.

The boundary term at the right chain end, $n = (L-1)/2$, is given by

$$\begin{aligned} \hat{B}_{2,\sigma} &= \cos(2\varphi) \left(\hat{C}_{(L-1)/2,\sigma}^+ \hat{C}_{(L-1)/2,\sigma} \right. \\ &\quad \left. - \hat{S}_{(L-1)/2,\sigma}^+ \hat{S}_{(L-1)/2,\sigma} \right) \\ &+ i \sin(2\varphi) \left(\hat{S}_{(L-1)/2,\sigma}^+ \hat{C}_{(L-1)/2,\sigma} - \text{h.c.} \right). \end{aligned} \quad (34)$$

The two chains are coupled at the right boundary via the term proportional to $\sin(2\varphi)$. The ring and two-chain geometries are shown in Fig. 1.

Note that the particle-hole transformation for the kinetic energy in the two-chain formulation is non-trivial,

$$\begin{aligned} \text{ph} : (-1)^n \hat{C}_{n,\sigma} &\mapsto \cos(\alpha_n) \hat{C}_{n,\sigma}^+ - i \sin(\alpha_n) \hat{S}_{n,\sigma}^+, \\ (-1)^n \hat{S}_{n,\sigma} &\mapsto \cos(\alpha_n) \hat{S}_{n,\sigma}^+ - i \sin(\alpha_n) \hat{C}_{n,\sigma}^+ \end{aligned} \quad (35)$$

with $\alpha_n = 2(n-1)\varphi$ for $n = 1, \dots, L-1$, and $\hat{c}_{0,\sigma} \mapsto \hat{c}_{0,\sigma}^+$ as before.

2. Chain separation

For large rings, the inter-chain coupling is small for three reasons. First, as seen from eq. (34), the chains for the C -electrons and S -electrons are coupled at a single site only, namely, at the right chain boundary, $n = (L-1)/2$. Second, in the SIAM the interesting physics happens at and around the origin, i.e., at the left boundary of the C -electron chain. Because of their large separation, we can expect that the right boundary at $n = (L-1)/2$ has little effect on the physics at the left boundary. Third, the inter-chain coupling vanishes

proportional to $\sin(2\varphi) \approx \pi/L$ for large rings. For these reasons, we set $\varphi \equiv 0$ in the following. Even quantities that are of order unity will show corrections of the order $1/L$ only.

The chain-separated SIAM reads

$$\hat{H} = \hat{H}^C + \hat{T}^S. \quad (36)$$

The undisturbed chain of anti-symmetric standing waves of length $(L-1)/2$ is described by

$$\begin{aligned} \hat{T}^S = & \frac{1}{4} \sum_{\sigma} \hat{S}_{(L-1)/2,\sigma}^+ \hat{S}_{(L-1)/2,\sigma}^- \\ & - \frac{1}{4} \sum_{n=1,\sigma}^{(L-3)/2} \left(\hat{S}_{n,\sigma}^+ \hat{S}_{n+1,\sigma}^- + \hat{S}_{n+1,\sigma}^+ \hat{S}_{n,\sigma}^- \right) \end{aligned} \quad (37)$$

with energy levels $\epsilon(k) = -\cos(k)/2$, $k = (2\pi/L)m_k$, $m_k = 1, 2, \dots, (L-1)/2$. The electrons on the chain of symmetric standing waves of length $(L+1)/2$ couple to the impurity at the origin,

$$\begin{aligned} \hat{H}^C = & \hat{H}_0^C + U \left(\hat{n}_{d,\uparrow} - \frac{1}{2} \right) \left(\hat{n}_{d,\downarrow} - \frac{1}{2} \right), \\ \hat{H}_0^C = & \hat{T}^C + \hat{V}, \\ \hat{T}^C = & -\frac{\sqrt{2}}{4} \sum_{\sigma} \left(\hat{C}_{0,\sigma}^+ \hat{C}_{1,\sigma}^- + \hat{C}_{1,\sigma}^+ \hat{C}_{0,\sigma}^- \right) \\ & - \frac{1}{4} \sum_{\sigma} \hat{C}_{(L-1)/2,\sigma}^+ \hat{C}_{(L-1)/2,\sigma}^- \\ & - \frac{1}{4} \sum_{n=1,\sigma}^{(L-3)/2} \left(\hat{C}_{n,\sigma}^+ \hat{C}_{n+1,\sigma}^- + \hat{C}_{n+1,\sigma}^+ \hat{C}_{n,\sigma}^- \right), \\ \hat{V} = & V \sum_{\sigma} \left(\hat{d}_{\sigma}^+ \hat{C}_{0,\sigma}^- + \hat{C}_{0,\sigma}^+ \hat{d}_{\sigma}^- \right), \end{aligned} \quad (38)$$

where we identified $\hat{c}_{0,\sigma} \equiv \hat{C}_{0,\sigma}$ to keep the notation consistent.

When we ignore the chain coupling term at the right boundary, we can factorize the ground state into the contributions from the chains C and S ,

$$|\Psi_0\rangle = |\Psi_0^C\rangle |\Psi_0^S\rangle, \quad (39)$$

where the upper index refers to the two commuting parts of the Hamiltonians for the C -electrons and S -electrons and $|\Psi_0^{C,S}\rangle$ are normalized to unity.

The mapping is advantageous for the DMRG treatment because we do not have to treat a ring geometry of L sites with periodic boundary conditions but a chain with $(L+1)/2 + 1$ sites where open boundary conditions apply. The C -electron chain has only about half as many sites as the ring which essentially doubles the system sizes that can be treated numerically for the ring geometry.

Note, however, that \hat{H}^C does not obey particle-hole symmetry for finite L but only in the thermodynamic limit. Deviations from particle-hole symmetry can be monitored by investigating the site occupancy of the impurity. Deviations from the exact value of one half, see eq. (19), can be used to quantify the violation of particle-hole symmetry, see Sect. V.

D. Spin correlation function

In this work we visualize the Kondo screening cloud for the single-impurity Anderson model. To this end, we calculate the spin correlation function between the impurity and bath sites.

1. Definition and general properties

Due to the spin-rotational invariance of the model it is sufficient to study the spin correlation function along the spin quantization axis. The local correlation function is defined by

$$\begin{aligned} C_{dd}^S = & \langle \Psi_0 | \hat{S}_d^z \hat{S}_d^z | \Psi_0 \rangle = \frac{1}{4} \langle \Psi_0 | (\hat{n}_{\uparrow}^d - \hat{n}_{\downarrow}^d)^2 | \Psi_0 \rangle \\ = & \frac{1}{4} - \frac{1}{2} \langle \Psi_0 | \hat{n}_{\uparrow}^d \hat{n}_{\downarrow}^d | \Psi_0 \rangle, \end{aligned} \quad (40)$$

where we used particle-hole symmetry (19) in the last step. The value for the on-site spin correlation interpolates between the itinerant limit, $C_{dd}(U=0) = 1/8$, and the atomic limit, $C_{dd}(W=0) = 1/4$.

The correlation function between the impurity site and the bath site r is defined by

$$\begin{aligned} C_{dc}^S(r) = & \langle \Psi_0 | \hat{S}_d^z \hat{S}_{r,c}^z | \Psi_0 \rangle \\ = & \frac{1}{4} \langle \Psi_0 | (\hat{n}_{\uparrow}^d - \hat{n}_{\downarrow}^d) (\hat{c}_{r,\uparrow}^+ \hat{c}_{r,\uparrow}^- - \hat{c}_{r,\downarrow}^+ \hat{c}_{r,\downarrow}^-) | \Psi_0 \rangle. \end{aligned} \quad (41)$$

Due to inversion symmetry we have

$$C_{dc}^S(L-r) = C_{dc}^S(r) \quad (42)$$

for $1 \leq r \leq (L-1)/2$.

To visualize the screening of the impurity spin, we define $\mathcal{S}(0) = C_{dd}^S + C_{dc}^S(0)$ and, for $R \geq 1$,

$$\mathcal{S}(R) = C_{dd}^S + C_{dc}^S(0) + \sum_{r=1}^R (C_{dc}^S(r) + C_{dc}^S(L-r)). \quad (43)$$

It describes the amount of the unscreened spin at distance R from the impurity site.¹⁸ The impurity is completely screened by all bath electrons. To see this we consider $\mathcal{S}((L-1)/2)$ on finite systems,

$$\begin{aligned} \mathcal{S}((L-1)/2) = & \langle \Psi_0 | \hat{S}_d^z \left(\hat{S}_d^z + \sum_{r=0}^{L-1} \hat{S}_{r,c}^z \right) | \Psi_0 \rangle \\ = & \langle \Psi_0 | \hat{S}_d^z \hat{S}^z | \Psi_0 \rangle = 0 \end{aligned} \quad (44)$$

because $|\Psi_0\rangle$ is an eigenstate of the operator \hat{S}^z for the total spin in z -direction with eigenvalue zero.

2. Spin correlations in two-chain geometry

For the first site of the chain we have

$$C_{dc}^S(0) = \frac{1}{4} \langle \Psi_0^C | (\hat{n}_{\uparrow}^d - \hat{n}_{\downarrow}^d) (\hat{C}_{0,\uparrow}^+ \hat{C}_{0,\uparrow}^- - \hat{C}_{0,\downarrow}^+ \hat{C}_{0,\downarrow}^-) | \Psi_0^C \rangle, \quad (45)$$

where we used eq. (39) and the normalization of $|\Psi_0^S\rangle$.

For the spin correlation function between the impurity site and a bath site at distance $1 \leq r \leq (L-1)/2$ we use inversion symmetry (42) to write

$$\begin{aligned} C_{dc}^S(r) &= \langle \Psi_0 | \hat{S}_d^z \hat{S}_r^z | \Psi_0 \rangle \\ &= \frac{1}{2} \langle \Psi_0 | \hat{S}_d^z \left(\hat{S}_r^z + \hat{S}_{L-r}^z \right) | \Psi_0 \rangle \\ &= \frac{1}{8} \langle \Psi_0^C | \left(\hat{n}_{\uparrow}^d - \hat{n}_{\downarrow}^d \right) \left(\hat{C}_{r,\uparrow}^+ \hat{C}_{r,\uparrow} - \hat{C}_{r,\downarrow}^+ \hat{C}_{r,\downarrow} \right) | \Psi_0^C \rangle, \end{aligned} \quad (46)$$

where we used the mapping onto the chain operators in the second step,

$$\hat{c}_{r,\sigma}^+ \hat{c}_{r,\sigma} + \hat{c}_{L-r,\sigma}^+ \hat{c}_{L-r,\sigma} = \hat{C}_{r,\sigma}^+ \hat{C}_{r,\sigma} + \hat{S}_{r,\sigma}^+ \hat{S}_{r,\sigma}, \quad (47)$$

and the factorization (39) in the last step; recall that the S -electron system is a paramagnetic Fermi sea, $\langle \Psi_0^S | \hat{S}_{r,\uparrow}^+ \hat{S}_{r,\uparrow} - \hat{S}_{r,\downarrow}^+ \hat{S}_{r,\downarrow} | \Psi_0^S \rangle = 0$.

Equations (45) and (46) must be evaluated using DMRG, in general. For $U = 0$, the ground-state energy and the spin correlation function can be evaluated analytically to a far extent, as we show next.

III. NON-INTERACTING SIAM

It is instructive to discuss the non-interacting SIAM. Moreover, it provides the basis for the Gutzwiller approach in Sect. IV. We defer the details of the derivation to the supplemental material²⁵ and merely summarize the relevant results.

A. Ground-state energy

The ground-state energy sums the band contribution and the energy of the doubly occupied bound state. The total energy reads²⁵

$$\begin{aligned} e_0(V) &= e_0^{\text{band}}(V) + e_0^b(V) \\ &= \frac{1}{2\pi} \left[-\pi + 2v_+ \arctan \left(\frac{1}{v_-} \right) \right. \\ &\quad \left. + v_- \ln \left(\frac{v_+ - 1}{v_+ + 1} \right) \right] + (1 - v_+), \end{aligned} \quad (48)$$

where

$$v_{\pm}(V) \equiv v_{\pm} = \frac{\sqrt{\sqrt{1+64V^4} \pm 1}}{\sqrt{2}}. \quad (49)$$

The small- V expansion becomes

$$e_0^{\text{small}}(V) = \frac{4V^2}{\pi} \left(\ln(V^2) + \ln(2) - 1 \right) - 4V^4. \quad (50)$$

Corrections are of the order $V^6 \ln(V^2)$. For $V = 0.1$, the approximate formula works very well. We have $e_0(0.1) = -0.06291$ whereas the approximation gives $e_0^{\text{small}}(0.1) = -0.06294$.

To determine the Gutzwiller variational energy we also need the derivative of the ground-state energy. We have

$$\begin{aligned} e_0'(x) &= \frac{4x}{\pi(v_+(x)^2 + v_-(x)^2)} \\ &\quad \left[2\pi v_-(x) \left(\frac{\arccot(v_-(x))}{\pi} - 1 \right) \right. \\ &\quad \left. + v_+(x) \ln \left(\frac{v_+(x) - 1}{v_+(x) + 1} \right) \right]. \end{aligned} \quad (51)$$

For small x this reduces to

$$e_0'(x \ll 1) \approx (8x/\pi) \ln(2x^2). \quad (52)$$

B. Magnetization and zero-field magnetic susceptibility

We introduce the magnetic energy scale $B_{\text{imp}} \equiv B = (g\mu_B/2)\mathcal{H}$ where \mathcal{H} is the external magnetic field at the impurity, and express the impurity magnetization $M(V, \mathcal{H}) = g\mu_B m(V, B)$ in terms of the impurity spin in z -direction,

$$m(V, B) = \langle \hat{S}_d^z \rangle = ((\hat{n}_{d,\uparrow} - \hat{n}_{d,\downarrow}))/2. \quad (53)$$

The magnetic susceptibility follows from

$$\chi(V, B) = \frac{\partial M(\mathcal{H})}{\partial \mathcal{H}} = \left(\frac{g\mu_B}{2} \right)^2 \frac{\partial [2m(V, B)]}{\partial B}. \quad (54)$$

We give closed expressions for $m(V, B)$ and $\chi(V, B)$ for the non-interacting SIAM in one dimension.

1. Magnetization

For the one-dimensional non-interacting SIAM we find for a magnetic field that acts solely at the impurity²⁵

$$\begin{aligned} 2m(V, B) &= Z[v_b(V, B)] - Z[v_b(V, -B)] \\ &\quad + \sum_{\sigma_n=\pm 1} \int_{-1/2}^0 \frac{d\omega}{\pi} \frac{\sigma_n \Gamma \sqrt{1-4\omega^2}}{(\omega + \sigma_n B)^2 (1-4\omega^2) + \Gamma^2} \end{aligned} \quad (55)$$

with $\Gamma = 2V^2$. Here, $v_b(V, B) < -1/2$ is the energy of the bound state outside the band. It is the root of $P_+(\omega, B)$, i.e., $P_+(v_b(V, B)) = 0$, with

$$P_+(\omega, B) = \omega + B + \frac{2V^2}{\sqrt{4\omega^2 - 1}}. \quad (56)$$

Moreover, the weight of the bound state in the d -electron spectral function is given by

$$Z[v_b(V, B)] = \left[1 - \frac{8V^2 v_b(V, B)}{(4[v_b(V, B)]^2 - 1)^{3/2}} \right]^{-1}. \quad (57)$$

In general, the magnetization must be determined numerically from eqs. (55) and (57).

2. Small hybridizations

In the limit $V \ll 1$, we ignore the bound-state contribution of order V^4 , and simplify the magnetization to

$$\begin{aligned} m(V, B) &= \int_{-\infty}^0 \frac{d\omega}{2\pi} \left[\frac{\Gamma}{(\omega + B)^2 + \Gamma^2} - \frac{\Gamma}{(\omega - B)^2 + \Gamma^2} \right] \\ &= \int_0^B \frac{d\omega}{\pi} \frac{\Gamma}{\omega^2 + \Gamma^2} = \frac{1}{\pi} \tan^{-1}(B/\Gamma). \end{aligned} \quad (58)$$

The width Γ of the d -electron spectral function is the relevant energy scale for magnetic excitations.

For small hybridizations, the susceptibility becomes

$$\chi(V, B) = \left(\frac{g\mu_B}{2} \right)^2 \frac{2}{\pi} \frac{\Gamma}{B^2 + \Gamma^2} \quad (59)$$

with the zero-field limit

$$\chi_0(V) = \left(\frac{g\mu_B}{2} \right)^2 \frac{2}{\pi\Gamma}. \quad (60)$$

As seen from Eq. (59), in the limit $V \rightarrow 0$ the magnetic susceptibility is proportional to the zero-field d -electron spectral function, $\mu(V, B) \propto D_{d,d,\sigma}(B)$.²⁵

3. External magnetic field for impurity and bath electrons

For the case $B_{\text{imp}} = B_{\text{bath}} \equiv B$, the bound states are shifted in energy,

$$v_b(V, B) = -B - v_+(V)/2, \quad (61)$$

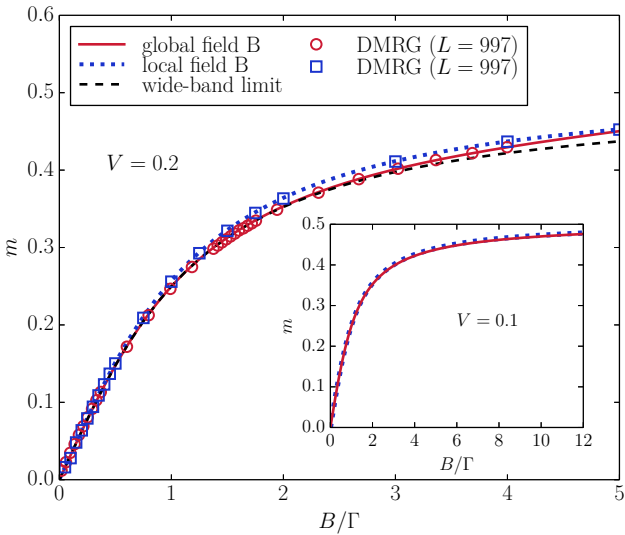


FIG. 2. (Color online) Impurity magnetization for the non-interacting symmetric SIAM for $V = 0.2$ as a function of $B = g\mu_B \mathcal{H}/2$. We show $m(0.2, B)$, eq. (55) (local field, blue dotted line), $\tilde{m}(0.2, B)$, eq. (62) (global field, red straight line), and the wide-band limit (58) (local field, black dashed line), together with the corresponding DMRG data (symbols, $L = 997$ sites). Inset: impurity magnetization for $V = 0.1$.

but their weights $Z[v_b(V, B)]$ do not change because $v_b(V, \pm B) \pm B = -v_+(V)/2$ in both cases. The rigid shift in single-particle energies by the magnetic field also guarantees that the impurity remains half filled on average for all external fields. The impurity magnetization becomes ($B \ll W$)

$$\begin{aligned} 2\tilde{m}(V, B) &= \sum_{\tau=\pm 1} \int_{-\infty}^0 \frac{V^2 \rho_0(\omega + \tau B)}{(\omega + \tau B)^2 + (\pi V^2 \rho_0(\omega + \tau B))^2} \\ &= 2 \int_0^B \frac{d\omega}{\pi} \frac{\Gamma \sqrt{1 - 4\omega^2}}{\omega^2(1 - 4\omega^2) + \Gamma^2}. \end{aligned} \quad (62)$$

For small hybridizations, $\tilde{m}(V, B)$ reduces to the result for $m(V, B)$ in eq. (58).

We show the impurity magnetization as a function of B/Γ in Fig. 2. Only for $V = 0.2$ and $B \gtrsim 2\Gamma$, there is a discernible difference between the curves for $m(0.2, B)$, eq. (55), where the external field is confined to the impurity, and $\tilde{m}(0.2, B)$, eq. (62), where the external field polarizes all electrons. In both cases, the DMRG data, see Sect. V, faithfully reproduce the analytic results, within small errors resulting from finite-size effects.

The wide-band limit closely follows the result for the global magnetic field. This indicates that the difference between applying the external field locally or globally is mostly due to the polarization of the bound-states for a local field. The bound states have a noticeable weight for $V = 0.2$.

Since the weight of the bound states is of the order V^4 , their contribution is much smaller for $V = 0.1$. Correspondingly, as seen from the inset of Fig. 2, the discrepancies between the magnetization curves for local and global external fields become very small. Since we shall work with $V \leq 0.1$ for the rest of the paper, we will restrict ourselves to purely local external magnetic fields, and shall safely ignore the influence of the magnetic field on the bath electrons.

C. Spin correlation function

1. General properties

Starting from eq. (41) we can use Wick's theorem and spin symmetry to show that

$$C_{dc}^S(r) = -\frac{1}{2} \left| \langle \Phi_0 | \hat{c}_{r,\uparrow}^+ \hat{d}_{\uparrow} | \Phi_0 \rangle \right|^2 \equiv -\frac{1}{2} M_r^2 \quad (63)$$

for the ground state $|\Phi_0\rangle$ of the non-interacting SIAM. The matrix element is calculated in the supplemental material,²⁵

$$\begin{aligned} M_r &= \sqrt{\frac{1}{L}} \sum_k e^{-ikr} \langle \Phi_0 | \hat{c}_{k,\uparrow}^+ \hat{d}_{\uparrow} | \Phi_0 \rangle \\ &= V \int_0^\pi \frac{dk}{\pi} \cos(kr) M[-\cos(k)/2], \end{aligned} \quad (64)$$

where we took the thermodynamic limit and used $\epsilon(k) = -\cos(k)/2$ in one dimension. Since $M(\epsilon)$ is real, particle-hole symmetry leads to $M(-\epsilon) = M(\epsilon)$ so that the matrix element vanishes for odd sites, $M_{2m-1} = 0$, $m \geq 1$. For even sites we find the bound-state and band contributions²⁵

$$M_{2m}^b = -\frac{2VZ(V)}{\sqrt{v_+^2 - 1}} \left(\sqrt{v_+^2 - 1} + v_+ \right)^{-2m}, \quad (65)$$

$$M_{2m}^{\text{band}} = -\frac{2V(-1)^m}{\pi} \int_0^\pi dy \frac{\cos(y/2)}{\sin^2(y) + 64V^4} \times [\sin(y) \cos(my) + 8V^2 \sin(my)]$$

with the pole frequency $\omega_b = -v_+/2$ and the pole weight

$$Z(V) = \frac{1}{1 + 4V^2 v_+ / v_-^3} \quad (66)$$

and v_\pm from eq. (49).

2. Small hybridizations

The bound-state contribution M_r^b is of the order V^3 for small V , and becomes exponentially small for $r \gg 1/(4V^2)$. For small V ,¹⁷ the band contribution is dominated by the region $y \rightarrow 0$ in the integrand in eq. (65). We thus approximate for small V

$$M_{2m} \approx -\frac{2V}{\pi} \int_0^\infty dx \frac{x \cos(8V^2 mx) + \sin(8V^2 mx)}{x^2 + 1} = (-1)^m \frac{2V}{\pi} e^\alpha \text{Ei}(-\alpha), \quad \alpha = 8V^2 m, \quad (67)$$

where

$$\text{Ei}(x) = - \int_{-x}^\infty dt \frac{e^{-t}}{t} \quad (68)$$

is the exponential integral. Thus, the spin correlation function approximately becomes ($m \neq 0$)

$$C_{dc}^S(2m) \approx -\frac{1}{2} \left(\frac{2V}{\pi} e^\alpha \text{Ei}(-\alpha) \right)^2, \quad \alpha = 8V^2 m. \quad (69)$$

In Figs. 3 and 4 we show the spin correlation function and the unscreened spin for the non-interacting symmetric SIAM in one dimension for $V = 0.1$. As seen from Fig. 3, the spin correlation function decays to zero proportional to $1/m^2$. The exact result (65) and the approximate formula (67) yield almost identical results, already for $m \geq 2$. For $m \geq 10$, the relative error is of the order 10^{-4} for $V = 0.1$.

Correspondingly, the unscreened spin shown in Fig. 4 decays to zero proportional to $1/m$. For small V , the screening is fairly inefficient and, correspondingly, the screening cloud extends very far into the host metal, even in the case of the non-interacting SIAM.

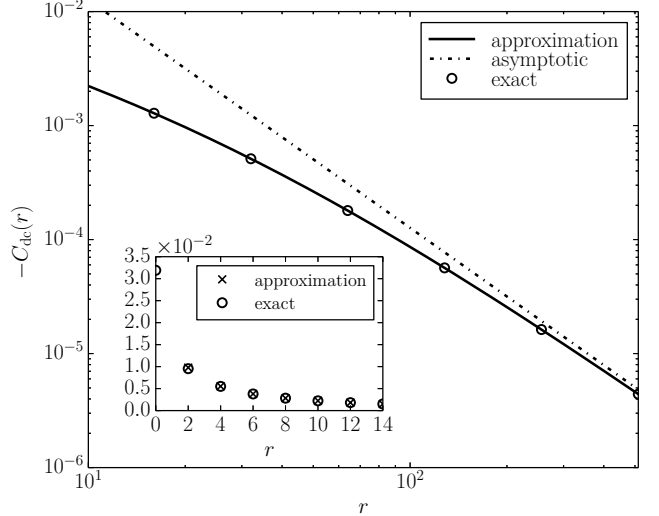


FIG. 3. Spin correlation function for the one-dimensional non-interacting symmetric SIAM for $V = 0.1$ (circles) on a log-log scale. The analytic result (69) is shown as a straight line. The asymptotics (70) is shown as dash-dotted line, and the exact values (65) are shown as open symbols. Inset: Spin correlation function for small distances on a linear scale.

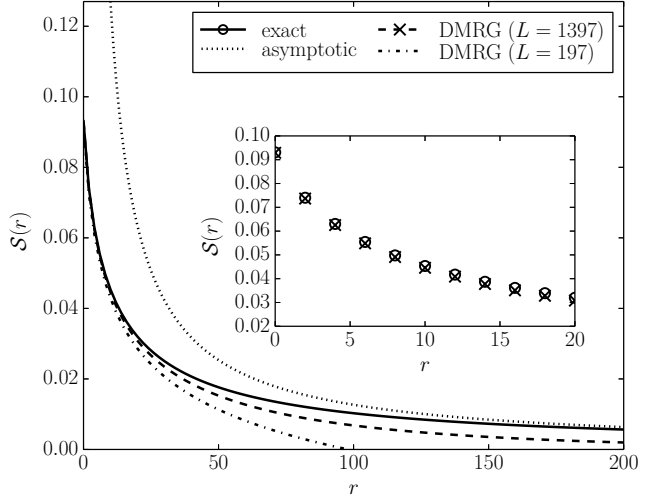


FIG. 4. Unscreened spin $S(r)$ at distance r from the impurity site, see eq. (43), for the one-dimensional non-interacting symmetric single-impurity Anderson model for $V = 0.1$. The analytic result based on eq. (69) is shown as a straight line. The asymptotic result (70) is presented by a dashed line. The DMRG data for $L = 197, 1397$ sites are given by dashed lines, see Sect. V. Inset: Unscreened spin for small distances, DMRG data for $L = 1397$ sites.

3. Small hybridizations and large distances

Here, we work out the long-range behavior of the spin correlation function. The asymptotic regime is reached for $\alpha \gg 1$, i.e., for $m \gg 1/(8V^2)$, where $\exp(\alpha)\text{Ei}(\alpha) \approx -1/\alpha$ in eq. (69). For the correlation function we find in

this region

$$C_{dc}^S(2m \gg 1/(4V^2)) \approx -\frac{1}{2} \left(\frac{2V}{\pi\alpha} \right)^2 = -\frac{1}{32\pi^2 V^2} \frac{1}{m^2}. \quad (70)$$

For the non-interacting symmetric SIAM in one dimension, the spin correlations between the impurity and a bath electron at site $2m$ asymptotically decays proportional to $1/(2m)^2$, see Fig. 3.

The matrix element M_{2m} at $\alpha = 1$ ($2m = 1/(4V^2)$) is already very small, of the order V^2 in the asymptotic region. Nevertheless, the contribution to the screening is finite even for $V \rightarrow 0$. The spins for $|m| > 1/(8V^2)$ ($\alpha > 1$) contribute approximately

$$\begin{aligned} \frac{\Delta S}{C_{dd}} &\approx 8 \left(\frac{2V}{\pi} \right)^2 \int_{1/(8V^2)}^{\infty} dm (e^\alpha \text{Ei}(-\alpha))^2 \\ &= \frac{4}{\pi^2} \int_1^{\infty} d\alpha (e^\alpha \text{Ei}(-\alpha))^2 \approx 0.23. \end{aligned} \quad (71)$$

The sites for $|m| > 1/(8V^2)$ contribute about 25% to the total screening of the spin at the impurity site where $C_{dd} = 1/8$.

Indeed, for large distances $r = 2m$ from the impurity, the unscreened spin decays only proportional to $1/r$,

$$S(r \gg 1) \sim \frac{1}{16\pi^2 V^2} \frac{1}{r}, \quad (72)$$

as follows from eq. (44) when we employ the Euler-Maclaurin formula for the asymptotic expression (70). This is shown in Fig. 4.

IV. GUTZWILLER VARIATIONAL APPROACH

In this section we define the Gutzwiller variational state and determine its variational parameters from minimizing the variational ground-state energy.^{23,24} Moreover, we determine the variational magnetization, zero-field susceptibility, and spin-spin correlation function between the impurity site and the host electrons.

A. Ground-state energy

1. Definition

The Gutzwiller wave function for the symmetric SIAM reads

$$\begin{aligned} |\Psi_G\rangle = & \left[\lambda_d (\hat{n}_\uparrow^d \hat{n}_\downarrow^d + (1 - \hat{n}_\uparrow^d)(1 - \hat{n}_\downarrow^d)) \right. \\ & \left. + \lambda_\sigma (\hat{n}_\uparrow^d (1 - \hat{n}_\downarrow^d) + (1 - \hat{n}_\uparrow^d) \hat{n}_\downarrow^d) \right] |\Phi_0\rangle, \end{aligned} \quad (73)$$

where $|\Phi_0\rangle$ is a normalized single-particle product state.

The Gutzwiller wave function is normalized,

$$\langle \Psi_G | \Psi_G \rangle = 1, \quad (74)$$

and symmetric,

$$\langle \Psi_G | \hat{n}_{d,\sigma} | \Psi_G \rangle = \frac{1}{2}, \quad (75)$$

if we use a symmetric single-particle product state,

$$\langle \Phi_0 | \hat{n}_{d,\sigma} | \Phi_0 \rangle = \frac{1}{2}, \quad (76)$$

and if we set

$$\lambda_d^2 = 1 - \sqrt{1 - q^2}, \quad \lambda_\sigma^2 = 2 - \lambda_d^2 = 1 + \sqrt{1 - q^2}. \quad (77)$$

Here, we introduced the remaining variational parameter $0 \leq q \leq 1$ that characterizes the Gutzwiller wave function.

2. Optimizing the variational parameters

The Gutzwiller variational ground-state energy with respect to the energy of the bare band is the minimum of

$$E_{\text{var}}(q) = e_0(qV) + \frac{U}{4} \left(1 - \sqrt{1 - q^2} \right) \quad (78)$$

over the variational parameter $0 \leq q \leq 1$. Here, $e_0(V)$ is the ground-energy of the non-interacting symmetric SIAM, \hat{H}_0 in eq. (2), see eq. (48). The minimum cannot be obtained analytically in general but we can derive an implicit equation.

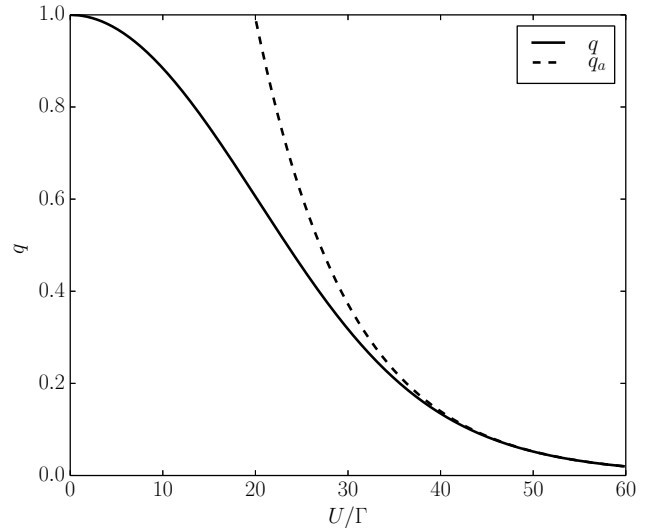


FIG. 5. Optimal Gutzwiller variational parameter as a function of U/Γ for $V = 0.1$ and the one-dimensional symmetric SIAM ($\Gamma = \pi d_0 V^2 = 2V^2$). The asymptotic result (80) is shown with a dashed line.

The minimization condition $(dE_{\text{var}}(q))/(dq) = 0$ leads to the equation

$$U(q, V) = -2\Gamma \sqrt{1 - q^2} e'_0(qV)/(qV) \quad (79)$$

with $\Gamma = \pi\rho_0(0)V^2 = \pi d_0 V^2 = 2V^2$ on a chain with nearest-neighbor hopping. Therefore, we know $U(q, V)$ for every $0 \leq q \leq 1$. The variational ground-state energy is thus given implicitly by eq. (78).

In Fig. 5 we show the Gutzwiller parameter as a function of U/Γ for $V = 0.1$, and compare to the analytic expression in the strong-coupling limit.

3. Strong coupling limit

For strong couplings, we find $q \rightarrow 0$ so that we may use the small- V expression to derive the variational ground-state energy analytically. Using eq. (52) in eq. (79) gives $q(U) \approx q_a(U)$ with

$$[q_a(U)]^2 = \frac{1}{\Gamma} \exp\left(-\frac{\pi U}{16\Gamma}\right), \quad (80)$$

and the variational ground-state energy becomes

$$E_{\text{opt}}(q \ll 1, V) \approx -\frac{2}{\pi} \exp\left(-\frac{\pi U}{16\Gamma}\right) \propto \exp\left(-\frac{1}{4d_0 J_K}\right) \quad (81)$$

with the Kondo energy $J_K = 4V^2/U$.

The ground-state energy becomes exponentially small, corresponding to the exponentially small Abrikosov-Suhl resonance in the spectral function.³ However, the Gutzwiller exponent is too small by a factor of two, $T_K \propto \exp[-1/(2d_0 J_K)]$,³ i.e., the Gutzwiller approach overestimates the width of the resonance. As seen from Fig. 5, for $V = 0.1$ the asymptotic behavior sets in around $U/\Gamma \approx 35$, for $q \lesssim 0.2$.

B. Magnetization and magnetic susceptibility

In the Gutzwiller variational approach, the impurity spin in z -direction is given by

$$m^G(V, B) = \frac{\lambda_\sigma^2}{2} \langle \Phi_0 | \hat{n}_{d,\uparrow} - \hat{n}_{d,\downarrow} | \Phi_0 \rangle \quad (82)$$

with λ_σ from eq. (77). Here, we keep a spin-dependent the q -factor and only consider the magnetic-field induced changes in the single-particle product state $|\Phi_0\rangle$. Therefore, the Gutzwiller variational result for the magnetization can be obtained from the non-interacting expression by replacing q by qV , see Sect. III B,

$$m^G(V, B) = (1 + \sqrt{1 - q^2}) m(qV, B). \quad (83)$$

The zero-field susceptibility in Gutzwiller theory reads

$$\chi_0^G(V, U) = (1 + \sqrt{1 - q^2}) \left(\frac{g\mu_B}{2}\right)^2 \frac{2}{\pi\Gamma} \frac{1}{q^2} \quad (84)$$

so that the variational Wilson ratio becomes

$$R^G(V, U) = \frac{\chi_0^G(V, U)}{\left(g\mu_B/2\right)^2 D_{d,d}^G(\omega = 0)} = 1 + \sqrt{1 - q^2}. \quad (85)$$

Here, we used the fact that the Gutzwiller approach describes a Fermi liquid where the density of states at the Fermi level is enhanced by a factor $1/q^2$. Eq. (85) shows that the Gutzwiller approach correctly reproduces the weak-coupling and strong-coupling limit, $R(U = 0) = 1$ and $R(U \gg \Gamma) = 2$. In the strong-coupling limit, the Wilson ratio deviates from two algebraically in $1/U$ due to the presence of charge fluctuations.³ In contrast, the Gutzwiller Wilson ratio is exponentially close to two because the Gutzwiller approach does not describe charge excitations properly.

For strong couplings, the zero-field susceptibility becomes

$$\Gamma\chi_0^G(V, u \gg 1) \approx \left(\frac{g\mu_B}{2}\right)^2 \frac{4\Gamma}{\pi} \exp\left(\frac{\pi u}{16}\right) \quad (86)$$

with $u = U/\Gamma$. The Gutzwiller approach correctly reproduces the exponentially large zero-field susceptibility for strong interactions, see Sect. V D.

C. Spin correlation function

1. Local correlation function

The spin correlation function on the impurity site reads

$$C_{dd}^S(q) = \frac{1}{4} - \frac{1}{2} \langle \Psi_0 | \hat{n}_{d,\uparrow} + \hat{n}_{d,\downarrow} | \Psi_0 \rangle = \frac{1}{4} - \frac{\lambda_d^2}{8} = \frac{1 + \sqrt{1 - q^2}}{8}. \quad (87)$$

The value for the on-site spin correlation correctly interpolates between the itinerant limit, $C_{dd}^S(q = 1) = 1/8$, and the atomic limit, $C_{dd}^S(q = 0) = 1/4$.

2. Correlation function between impurity and bath sites

We continue with the spin correlation function between the impurity site and a bath site at distance r ,

$$C_{dc}^S(q, r) = \frac{1 + \sqrt{1 - q^2}}{4} \langle \Phi_0 | \left(\hat{d}_{\uparrow}^+ \hat{d}_{\uparrow} - \hat{d}_{\downarrow}^+ \hat{d}_{\downarrow} \right) \left(\hat{c}_{r,\uparrow}^+ \hat{c}_{r,\uparrow} - \hat{c}_{r,\downarrow}^+ \hat{c}_{r,\downarrow} \right) | \Phi_0 \rangle = -\frac{1 + \sqrt{1 - q^2}}{2} \left| \langle \Phi_0 | \hat{c}_{r,\uparrow}^+ \hat{d}_{\uparrow} | \Phi_0 \rangle \right|^2, \quad (88)$$

where we applied spin symmetry and Wick's theorem in the last step. The matrix element is evaluated in Sect. III C, and we merely have to replace $V \rightarrow (qV)$ in all expressions there.

V. INTERACTING SIAM

In this section we compare our Gutzwiller variational results to those from the DMRG method that provides

essentially exact numerical data for the SIAM on large rings. For comparison we also include results from magnetic Hartree-Fock theory, as derived in the supplemental material,²⁵ and compare to the ground-state energy from the Bethe Ansatz solution.³⁰

A. DMRG Method

We study the symmetric SIAM in the effective single-chain representation (38) using the DMRG method. In contrast to previous applications of the canonical transformation to the standard one-dimensional Hubbard model, in the present case the mapping leads to a substantial gain over standard implementations in numerical simulations.²⁶ The mapping leads to an effective system size that is about half of the ring size, and it provides open boundary conditions that are more favorable for the DMRG method than periodic boundary conditions.^{31,32}

1. Technicalities

We study the effective Hamiltonian of C -electrons on a chain up to system 700 sites that corresponds to $L = 1397$ in the ring geometry. This allows us to study systems with periodic boundary conditions that are three times longer than used in previous studies with open boundary conditions.¹⁸ The accuracy of the calculations is controlled using the dynamic block-state selection (DBSS) scheme.^{33,34} Setting the control parameter to $\chi = 10^{-5}$, the truncation error yields around 10^{-7} while the number of maximally kept DMRG block-states can grow up to $M = 5000$ for large system sizes. For strong interactions, we target multiple states to stabilize convergence.

On finite lattices, the calculation of the magnetization as a function of a globally applied field \mathcal{H} is more subtle because S^z is a good quantum number. Therefore, the spin quantum number S^z changes from $S^z = 0$ for $\mathcal{H} = 0$ to $S^z = 1, 2, 3, \dots$ for increasing external fields in steps of $g\mu_B \mathcal{H}_n$ when

$$g\mu_B \mathcal{H}_n = E_0(S^z = n) - E_0(S^z = n - 1) \quad (89)$$

for $n = 1, 2, 3, \dots$. Thus, the impurity magnetization $\tilde{m}(V, B)$ is recorded only at discrete values of the external field whereby expectation values are calculated with the ground state for $S^z = n$. Since the energy differences are of the order $1/L$, the smallest accessible magnetic energy scale is of the order W/L . In this work, we include only the results for $U = 0, V = 0.2$, see Fig. 2, to demonstrate the applicability of the approach.

For most of the results below, we apply the magnetic field only at the impurity. Since \hat{P} in the Hamiltonian (2) is not conserved, standard DMRG ground-state calculations provide the results for the impurity magnetization.

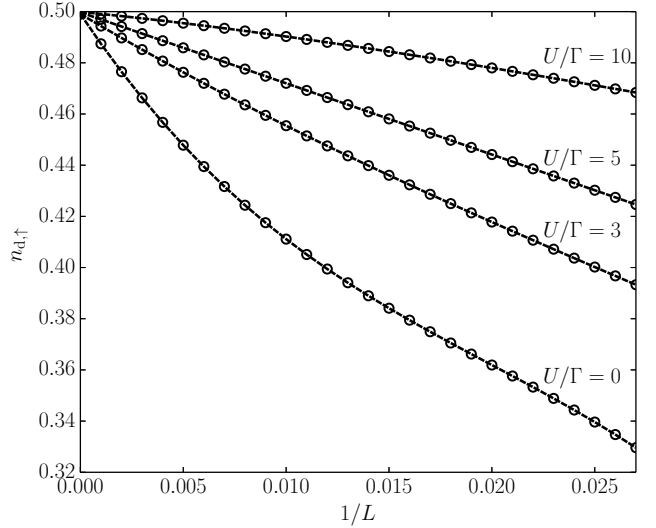


FIG. 6. DMRG results for the impurity occupation $n_{d,\sigma}$ of the open-chain SIAM as a function of inverse system size $1/L$ for various values of U/Γ and $V = 0.1$ ($\Gamma = \pi d_0 V^2 = 2V^2$). Lines are only guides to the eyes.

2. Tests

To test the accuracy of our open-chain approach, in Fig. 6 we show the finite-size scaling of the impurity occupancy $n_{d,\sigma}(L) = \langle \hat{n}_{d,\sigma} \rangle$ for the open-chain SIAM (38) for various values of U/Γ at $V = 0.1$. It is seen that the occupation extrapolates to its value in the presence of particle-hole symmetry, $n_{d,\sigma}(\infty) = 1/2$. For $U > 0$, the electrons repel each other on the impurity. Thus, the Hubbard interaction suppresses charge fluctuations and shifts $n_{d,\sigma}(L)$ towards one half already at small system sizes.

As another test, we present the ground-state energy $\Delta E_0(U, V)$ as a function of inverse system size for $V = 0.1$ and various values of the interaction strength U/Γ in Fig. 7. Here, we measure the ground-state energy with respect to the case $V = 0$,

$$\Delta E_0(U, V) = E_0(U, V) - E_0(U, 0), \quad (90)$$

i.e., we subtract the band contribution of the free host electrons and the term $-U/4$ for the singly occupied impurity site. Therefore, $\Delta E_0(U, V)$ is of the order unity and tends to zero for large interaction strengths. Using a second-order polynomial fit in the inverse system size, the DMRG energies extrapolated to the thermodynamic limit coincide with the values from Bethe Ansatz. Note that the Bethe Ansatz approach covers the wide-band limit, $U \ll W$, and also ignores corrections of order V^4 . Therefore, the extrapolated DMRG energies are slightly below the Bethe-Ansatz energies.

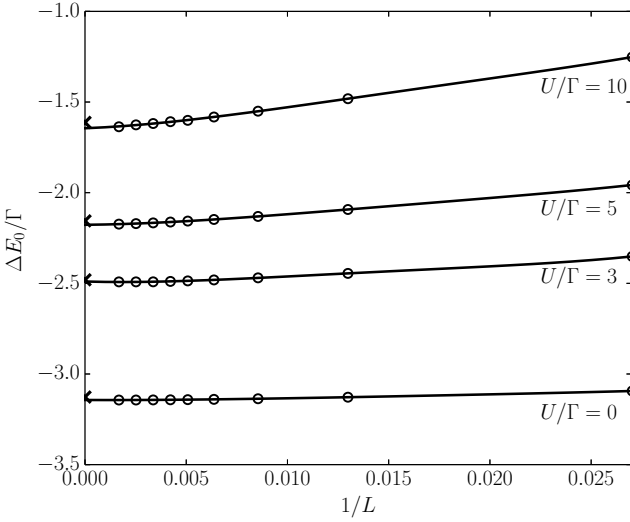


FIG. 7. DMRG result for the ground-state energy $\Delta E_0(U, V)$ of the one-dimensional symmetric SIAM as a function of inverse system size $1/L$ for various values of U/Γ and $V = 0.1$ ($\Gamma = \pi d_0 V^2 = 2V^2$). The crosses denote the values from the Bethe Ansatz, becoming exact in the wide-band limit. The solid lines represent the second-order polynomial fit.

B. Ground-state energy

1. Small interaction strengths

For the symmetric SIAM, the ground-state energy is known for weak coupling, $U \ll \pi\Gamma$,^{3,35}

$$\Delta E_0(U, V) = e_0(V) + \frac{U}{4} + \pi\Gamma \sum_{n=1}^{\infty} (-1)^n e^{(2n)}(V) \left(\frac{U}{\pi\Gamma} \right)^{2n} \quad (91)$$

where $\Gamma = \pi d_0 V^2 = 2V^2$. Due to particle-hole symmetry, there are no odd-order corrections in the weak-coupling series beyond the Hartree term.

For $V \ll 1$, $e^{(2n)}(V)$ weakly depends on V . We find (see supplemental material)

$$\begin{aligned} e^{(2)}(0.1) &= 0.0374447, \\ e^{(2)}(0.05) &= 0.0369271, \end{aligned} \quad (92)$$

in very good agreement with the analytical result obtained by Yamada,³⁵

$$e^{(2)}(V=0) = \frac{1}{4} - \frac{7}{4\pi^2} \zeta(3) \approx 0.0368608. \quad (93)$$

Moreover, the fourth-order coefficient is known to be very small, $e^{(4)}(V=0) \approx 0.0008$.³⁵

The Gutzwiller approach leads to

$$e_G^{(2)}(V) = \frac{\pi\Gamma}{[-32V e'_0(V)]} \approx -\frac{\pi^2}{128 \ln(2V^2)}. \quad (94)$$

In contrast to the exact expression, the prefactor of the second-order term vanishes logarithmically for $V \rightarrow 0$.

For $V = 0.1$, we find $e_G^{(2)}(0.1) = 0.01943$, about half of the exact value in eq. (92). The paramagnetic Fermi sea remains the Hartree-Fock ground state until magnetic order sets in at about $U_{c,\text{HF}} \approx \pi\Gamma$. Therefore, there is no second-order term in the ground-state energy in Hartree-Fock theory.

2. Wide-band limit

For small hybridizations and $V \ll U \ll W$, the SIAM can be solved analytically using the Bethe Ansatz because the dispersion relation of the host electrons can be linearized around the Fermi wave vector.^{19–22} For the symmetric SIAM in the absence of a magnetic field, the ground-state energy can be calculated analytically,³⁰

$$\frac{\Delta E_0^{\text{BA}}(U_{\text{BA}}, V_{\text{BA}})}{t_{\text{BA}}} = \frac{U_{\text{BA}}}{2} + \int_{-\infty}^A d\Lambda 2x(\Lambda) \sigma_S(\Lambda) \quad (95)$$

with

$$\begin{aligned} x(\Lambda) &= -\frac{\sqrt{2}}{2} \sqrt{\Lambda + \sqrt{\Lambda^2 + U_{\text{BA}}^2 V_{\text{BA}}^4/4}}, \\ \sigma_S(\Lambda) &= \int_{-\infty}^{\infty} \frac{dk}{4\pi} \frac{V_{\text{BA}}^2}{(k + U_{\text{BA}}/2)^2 + V_{\text{BA}}^4/4} \\ &\quad \times \frac{1}{U_{\text{BA}} V_{\text{BA}}^2} \text{sech} \left[\frac{\pi(k^2 - \Lambda)}{U_{\text{BA}} V_{\text{BA}}^2} \right], \end{aligned} \quad (96)$$

where $\text{sech}(x) = 1/\cosh(x)$ is the hyperbolic secant function. The energy shift $U_{\text{BA}}/2$ takes our definition into account that $\Delta E_0(U, V)$ is measured with respect to the limit of vanishing hybridization, $\Delta E_0^{\text{BA}}(U, 0) = 0$.

Note that in eq. (96) all energies are expressed in units of t_{BA} so that the Fermi velocity is $v_F^{\text{BA}} = t_{\text{BA}}$. In our energy units we have $v_F = W/2$ so that we must set $t_{\text{BA}} = W/2 \equiv 1/2$, i.e., we must scale all energies by a factor of two. Moreover, in the Hamiltonian used in the Bethe Ansatz, only the symmetric linear combination of right-movers and left-movers couples to the impurity whereas the hybridization in the lattice Hamiltonian (5) is expressed in terms of left-movers and right-movers. This implies $V_{\text{BA}}/t_{\text{BA}} = 2\sqrt{2}V/W$ and $U_{\text{BA}} = 2U/W$ in our energy units.

We adjust the bandwidth cutoff-parameter A to reproduce the ground-state energy (50) of the non-interacting SIAM to orders $V^2 \ln(V^2)$ and V^2 . For $A = 2e$ we indeed find $\Delta E_0^{\text{BA}}(0, V) = (4V^2/\pi)[\ln(V^2) + \ln(2) - 1] + \mathcal{O}(V^4)$, see eq. (50).

Ignoring terms of order V^4 and higher that are beyond the wide-band limit, the ground-state energy reads

$$\begin{aligned} \frac{\Delta E_0^{\text{BA}}(U, V)}{\Gamma} &= \frac{u}{2} + \sum_{\sigma} \int_{-e/\Gamma}^0 \frac{dp}{\pi} \frac{1}{(p + \sigma_n u/2)^2 + 1} \\ &\quad \times \int_{-\infty}^{\infty} \frac{dy}{\pi} \text{sech}(y) \tilde{x}(p^2 - 2uy/\pi, u), \\ \tilde{x}(\lambda, u) &= \frac{\sqrt{2}}{2} \sqrt{\lambda + \sqrt{\lambda^2 + u^2}} \end{aligned} \quad (97)$$

with $\Gamma = 2V^2$ and $u = U/\Gamma$. These expressions are amenable to a numerical evaluation of the integrals.

To extract the limiting behavior and to show the equivalence with the Hartree-Fock energy for $U/\Gamma \gg 1$, we write

$$\Delta E_0^{\text{BA}}(U, V) = \Delta E_0^{\text{BA},1}(U, V) + \Delta E_0^{\text{BA},2}(U, V), \quad (98)$$

where

$$\frac{\Delta E_0^{\text{BA},1}(U, V)}{\Gamma} = \frac{u}{2} + \sum_{\sigma} \int_{-e/\Gamma}^0 \frac{dp}{\pi} \frac{p}{(p + \sigma_n u/2)^2 + 1} \quad (99)$$

and

$$\frac{\Delta E_0^{\text{BA},2}(U, V)}{\Gamma} = \sum_{\sigma} \int_{-\infty}^0 \frac{dk}{\pi} \frac{u}{(k\sqrt{u} + \sigma_n u/2)^2 + 1} \times \int_{-\infty}^{\infty} \frac{dy}{\pi} \text{sech}(y) X(k^2 - 2y/\pi) \quad (100)$$

with

$$X(\lambda) = -k + \frac{\sqrt{2}}{2} \sqrt{\lambda + \sqrt{\lambda^2 + 1}}. \quad (101)$$

The second term gives for $u \gg 1$

$$\frac{\Delta E_0^{\text{BA},2}(U \gg \Gamma, V)}{\Gamma} = \frac{\pi}{u} + \mathcal{O}(1/u^2). \quad (102)$$

The first term is equivalent to the Hartree-Fock expression in the limit $m \rightarrow 1/2$ that is reached for $U/\Gamma \gg 1$, see supplemental material.²⁵ Moreover, the integral is readily evaluated and gives in the intermediate coupling regime ($\Gamma = 2V^2/W \ll U \ll W$)

$$\frac{\Delta E_0^{\text{BA},1}(U, V)}{\Gamma} = \frac{2}{\pi} \ln(\Gamma/e) + \frac{u}{2} \left(1 - \frac{2}{\pi} \tan^{-1}(u/2) \right) + \frac{1}{\pi} \ln(1 + u^2/4). \quad (103)$$

It is seen that the ground-state energy increases logarithmically, i.e., as a function of $\ln(u)$, in the intermediate coupling regime.³⁰

One may wonder whether or not the Kondo energy scale can be extracted from the Bethe-Ansatz energy expression (97). Indeed, the region $[(p + u/2) \leq \nu_1, |y - p^2\pi/(2u)| \leq \nu_2]$ with $\nu_{1,2}$ of order unity gives rise to a contribution of the order of

$$T_L(U) = \Gamma \sqrt{\frac{u}{2}} \exp \left[-\frac{\pi u}{8} + \frac{\pi}{2u} \right] \quad (104)$$

with $u = U/\Gamma$. $T_L(U)$ is proportional to the Kondo temperature for the symmetric SIAM in the strong-coupling limit.³ Note, however, that the integration over all (p, y) region wipes out this term in the ground-state energy. It is only in magnetic properties that the energy scale T_L becomes visible,³ see Sect. V C.

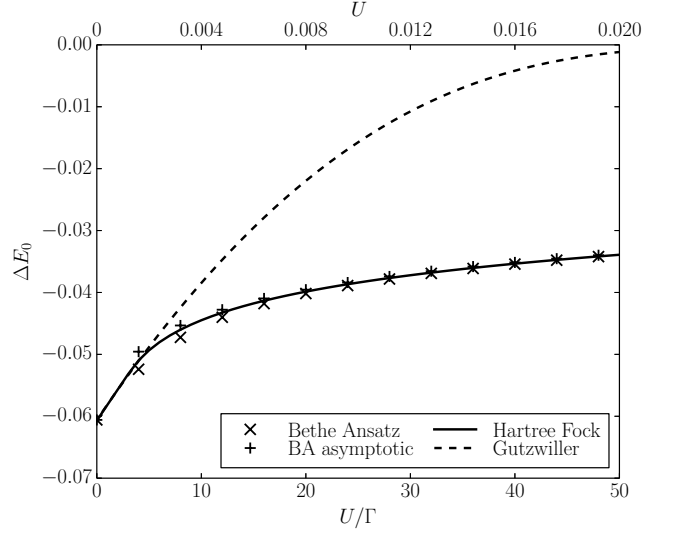


FIG. 8. Ground-state energy $\Delta E_0(U, V)$ for the symmetric SIAM in one dimension as a function U/Γ for $V = 0.01$ ($\Gamma = \pi d_0 V^2 = 2V^2 = 0.0002$). The full (dashed) lines display the Hartree-Fock (Gutzwiller) variational upper bound, the open symbols give the Bethe Ansatz results from eq. (97), and the crosses denote the asymptotic result (103).

3. Comparison

In Fig. 8 we compare the Gutzwiller, Hartree-Fock, and Bethe Ansatz energies for $V = 0.01$ ($\Gamma = 0.0002$). For such small hybridizations, DMRG calculations would require system sizes that are an order of magnitude larger because even at $U = 0$ the relevant energy scale $\Gamma = 2V^2/W$ becomes very small. In Fig. 9 we show the ground-state energies for $V = 0.1$ ($\Gamma = 0.02$) from weak-coupling perturbation theory, Gutzwiller, Hartree-Fock, finite-size extrapolated data from DMRG, and Bethe Ansatz. Since the Bethe Ansatz approach covers the wide-band limit, $U \ll W$, the extrapolated DMRG energies and the Hartree-Fock energies lie below the Bethe-Ansatz energies, as becomes discernible at $V = 0.1$ for $U/\Gamma \gtrsim 10$ in Fig. 9.

As seen from the two figures, the Gutzwiller energy curve deviates noticeably from the exact results for $U/\Gamma > 10$. Like second-order perturbation theory, it provides a good estimate only for $U \lesssim 5\Gamma$. At large interactions, the Gutzwiller variational energy becomes exponentially small. Since the wave function does not properly describe charge fluctuations, i.e., the Hubbard bands, the Gutzwiller variational energy bound is poor.

In Hartree-Fock theory, a magnetic moment is formed only for $U_c^{\text{HF}} \approx \pi\Gamma$, and the ground-state energy contains a cusp at U_c . More importantly, above $U \approx 5\Gamma$ the Hartree-Fock theory provides an excellent bound on the exact ground-state energy. For small hybridizations, the exact Bethe-Ansatz and DMRG energies are in almost perfect agreement with the Hartree-Fock upper bounds. Since the quasi-particle peak provides an exponentially

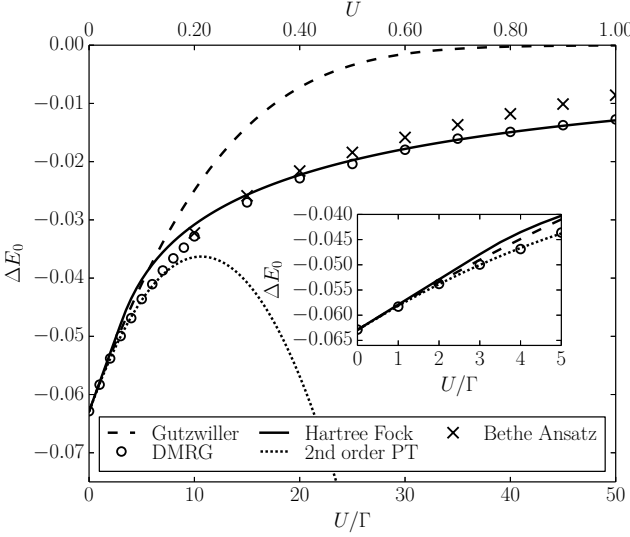


FIG. 9. Ground-state energy $\Delta E_0(U, V)$ for the symmetric SIAM on a ring as a function U/Γ for $V = 0.1$ ($\Gamma = \pi d_0 V^2 = 2V^2 = 0.02$). The second-order weak-coupling result (92) is shown as a short-dashed line, the full (dashed) lines display the Hartree-Fock (Gutzwiller) variational upper bound, the open symbols are the DMRG data, extrapolated to the thermodynamic limit, and the crosses give the Bethe Ansatz values. Inset: ground-state energy for small interaction strengths.

small energy contribution for $U \gg \Gamma$, the energy is solely determined by the lower Hubbard band which gives rise to a $\ln(u)$ increase of the ground-state energy, see eq. (103). The result for $\Delta E_0^{\text{BA},1}(U, V)/\Gamma$ is also shown in Fig. 8.

Obviously, the lower Hubbard band for $u \gg 1$ is perfectly described by Hartree-Fock theory. Therefore, Hartree-Fock theory provides an excellent starting point for analytical theories like the Local Moment Approach that covers both the high-energy and low-energy parts of the single-particle spectrum.¹⁰⁻¹²

C. Magnetization and magnetic susceptibility

The Bethe Ansatz permits the exact calculation of the impurity magnetization in the presence of a magnetic field on the impurity. Hereby, it is implicitly understood that the effect of the magnetic field on the conduction electrons is negligibly small so that it does not make a difference whether or not the magnetic field is also applied to the bath electrons.

1. Magnetization

The analysis of the Bethe Ansatz equations depends on the value of the external field $b = B/\Gamma$. First, region I, $b \leq b_0(u)$, covers the weak-field regime $b \rightarrow 0$ and the

Kondo regime for $u \gg 1$. Region II, $b \geq b_0(u)$, covers the large-field regime $b \rightarrow \infty$. The magnetization and the magnetic susceptibility are continuous at $b = b_0(u)$. The boundary value is determined by ($\ln(e) = 1$)

$$b_0(u) = \sqrt{2u} \frac{1}{\sqrt{\pi}} \sum_{n=0}^{\infty} \frac{1}{n!} \left(\frac{2n+1}{2e} \right)^{n+1/2} \frac{1}{(2n+1)^{3/2}} \approx 0.398942\sqrt{2u}. \quad (105)$$

For $u \rightarrow 0$, only region II exists, whereas in the Kondo limit, for $u \rightarrow \infty$, only region I remains.

a. *Magnetization in region I:* The magnetization and the magnetic field parametrically depend on each other. For $p \geq 0$, Tsvelik and Wiegmann give²¹

$$b_I(p, u) = \sqrt{\frac{2u}{\pi}} \sum_{n=0}^{\infty} \frac{1}{n!} \left(\frac{2n+1}{2e} \right)^{n+1/2} \frac{e^{-\pi(2n+1)p}}{(2n+1)^{3/2}} \quad (106)$$

for the applied magnetic field so that $b_I(0, u) = b_0(u)$.

The impurity magnetization contains two terms,

$$m_I(p, u) = m_K(p, u) + m_{\text{reg}}(p, u), \quad (107)$$

namely, the ‘Kondo term’ $m_K(p, u)$ and the ‘regular term’ $m_{\text{reg}}(p, u)$. We discuss them separately.

The Kondo term is given by ($\eta = 0^+$),^{21,36}

$$m_K(p, u) = \frac{(-i)}{4\pi^{3/2}} \int_{-\infty}^{\infty} \frac{d\omega}{\omega - i\eta} \left(\frac{i\omega + \eta}{e} \right)^{i\omega} \Gamma \left(\frac{1}{2} - i\omega \right) \times \exp [-2\pi i\omega(p - J^{-1}(u))] , \quad (108)$$

where

$$J^{-1}(u) = \frac{u^2 - 4}{8u} \quad (109)$$

is the inverse Kondo coupling, and $\Gamma(x)$ denotes the Gamma function. The Kondo contribution cannot be obtained in weak-coupling perturbation theory because of the $1/u$ -singularity in the exponent. Moreover, it gives rise to a diverging zero-field susceptibility for $u \gg 1$, see Sect. V C 2 below.

The regular contribution reads

$$m_{\text{reg}}(p, u) = \frac{1}{\sqrt{\pi}} \sum_{n=0}^{\infty} \frac{1}{n!} \left(\frac{2n+1}{2e} \right)^{n+1/2} \frac{e^{-\pi p(2n+1)}}{2n+1} \times F \left(\frac{\pi(2n+1)}{2u}, u \right) \quad (110)$$

with

$$\begin{aligned} F(a, u) &= \int_{-\infty}^{\infty} \frac{dy}{\pi} e^{-ay^2} \frac{1}{1 + (iy + u/2)^2} \\ &= \int_0^{\infty} \frac{2dy}{\pi} e^{-ay^2} \frac{1 - y^2 + u^2/4}{u^2 y^2 + (1 - y^2 + u^2/4)^2} \\ &= e^{-a(1-u^2/4)} \int_0^a \frac{dx}{\sqrt{\pi x}} \exp \left[x - \frac{a^2 u^2}{4x} \right] \end{aligned} \quad (111)$$

with the analytic expression

$$F(a, u) = -e^{-a(1-u^2/4)} \sin(au) + e^{-a(1-u^2/4)} \operatorname{Re} [e^{iau} \operatorname{Erfi}(\sqrt{a}(2-iu)/2)] , \quad (112)$$

where $\operatorname{Erfi}(x)$ is the complex error function. The analytic formula is helpful for the derivation of series expansions of $F(a, u)$ for small and large arguments a .

b. *Magnetization in region II:* For the applied magnetic field, Tsvelik and Wiegmann give²¹

$$b_{II}(p, u) = b_0(u) + \sqrt{\frac{u}{4\pi}} \int_0^\infty \frac{dx}{x^{3/2}} \frac{(1-e^{-2\pi px})}{\Gamma(\frac{1}{2}+x)} \left(\frac{x}{e}\right)^x \quad (113)$$

for $p \geq 0$. The magnetization in region II is given by

$$m_{II}(p, u) = \frac{1}{2} - \frac{1}{2} \int_0^\infty \frac{dx}{\sqrt{\pi x}} \frac{e^{-2\pi px}}{\Gamma(\frac{1}{2}+x)} \left(\frac{x}{e}\right)^x F\left(\frac{\pi x}{u}, u\right) . \quad (114)$$

As shown in the supplemental material,²⁵ the result for the non-interacting SIAM is readily recovered from eqs. (113) and (114). There, we also derive an explicit formula for the large-field limit,

$$m_{II}(b \gg \sqrt{u/\pi}) \approx \frac{1}{2} - \frac{1}{\pi b} + \frac{u}{2\pi b^2} + \frac{4\pi - 12u - 3\pi u^2}{12\pi^2 b^3} \quad (115)$$

up to and including all terms of the order $1/b^3$, and the low-energy Kondo scale $T_L(U)$ is absent for large fields.

In fact, there are no logarithmic terms to all orders of the $1/b$ expansion because, for $b \gg 1$, both $b(p, u)$ and $m_{II}(p, u)$ can be expressed in terms of a series with odd powers in the parameter $1/\sqrt{z}$ where z obeys $p = z - \ln(2\pi e z)/(2\pi)$.²¹ Therefore, at large values of the external field, the impurity magnetization does not show any signs of the logarithmic Doniach-Šunjić-Hamann tails in the impurity spectral function.^{10-12,37}

We show the impurity magnetization as a function of the local external field for small and moderate interactions strengths in Fig. 10 and Fig. 11, respectively. The DMRG reproduces the magnetization curves very well, particularly at strong magnetic fields. DMRG requires very large system sizes to resolve the steep initial slope of the magnetization curves, especially for moderate to large interaction strengths. This behavior is reflected in the zero-field susceptibility that becomes exponentially large for large interactions in an exponentially narrow region of external fields, as we discuss next.

2. Zero-field magnetic susceptibility

For $b_I(p, u) \equiv b \rightarrow 0$, we have $p \rightarrow \infty$ in eq. (106) so that we only retain the first term in the series. Thus,

$$p = -\frac{1}{\pi} \ln \left(b \sqrt{\frac{\pi e}{u}} \right) \gg 1 . \quad (116)$$

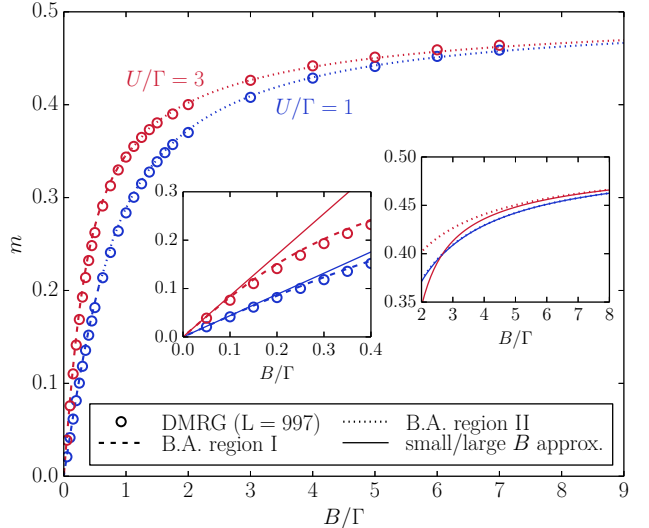


FIG. 10. (Color online) Impurity magnetization $m(V = 0.1, B) = \langle \hat{S}_d^z \rangle$ as a function of the external magnetic field $b = B/\Gamma = g\mu_B \mathcal{H}/(2\Gamma)$ for weak interactions, $u = U/\Gamma = 1, 3$, from the Bethe Ansatz for the symmetric SIAM. The insets show the behavior for small and large fields with the small-field asymptotics (118) and the large-field asymptotics (115). The circles are DMRG results for rings with $L = 997$ sites.

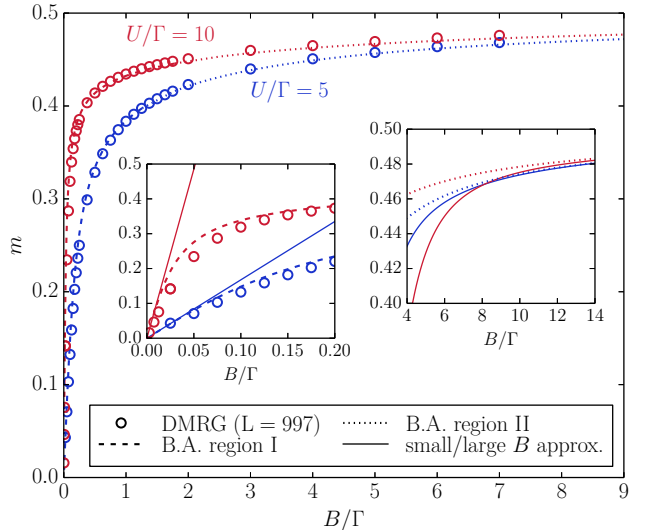


FIG. 11. (Color online) Same as Fig. 10 for moderate couplings $u = 5, 10$.

For the case $[p - J^{-1}(u)] \geq 0$, we may represent $m_K(p, u)$ in terms of a sum by performing a contour integral in the lower complex ω -plane,

$$m_K(p, u) = \frac{1}{\sqrt{\pi}} \sum_{n=0}^{\infty} \frac{(-1)^n}{2n+1} \frac{1}{n!} \left(\frac{2n+1}{2e} \right)^{n+1/2} \times \exp [-\pi(p - J^{-1}(u))(2n+1)] . \quad (117)$$

In this sum for the Kondo contribution and in the sum for the regular contribution, eq. (110), we keep only the first term in the series and find ($m_I(p, u) \equiv m(b, u)$)

$$m(b \rightarrow 0, u) \approx \frac{b}{\sqrt{2u}} e^{\pi/J(u)} \left(1 + e^{-\pi/J(u)} F(\pi/(2u), u) \right) \quad (118)$$

for small b , with corrections of the order b^3 .²¹

Thus, the Bethe Ansatz provides an explicit expression for the impurity susceptibility in the wide-band limit,^{3,21,38}

$$\chi_0^{\text{BA}}(U, V) = \left(\frac{g\mu_B}{2} \right)^2 \frac{1}{T_L(U)} \left[1 + \int_0^{\pi/(2u)} \frac{dx}{\sqrt{\pi x}} \exp \left(x - \frac{\pi^2}{16x} \right) \right] \quad (119)$$

with $u = U/\Gamma$ and $T_L(U)$ from eq. (104). Since the integral vanishes for $u \rightarrow \infty$, the exponential term gives the result in the Kondo limit.

We show the zero-field susceptibility in Fig. 12. As seen from eqs. (104) and (119), the zero-field susceptibility increases exponentially as a function of u . This behavior is difficult to reproduce in DMRG because, as the magnetization is bounded from above, the magnetic-field region where the susceptibility is exponentially large is exponentially small. Therefore, it is hard to calculate the zero-field susceptibility for $u \gtrsim 10$ from DMRG. For $u = 10, 15$ we choose $B = 0.0025\Gamma$ and calculate $\chi_0^{\text{DMRG}}(U, V = 0.1) = (g\mu_B/2)^2[2m(B, u)/B]$. As seen from Fig. 12, the agreement between the Bethe Ansatz results and DMRG is very good for $u \lesssim 10$, and quite acceptable for $u \lesssim 15$ where the zero-field susceptibility is enhanced by more than a factor of 100 over its non-interacting value.

The Gutzwiller variational theory reproduces the exponential behavior of the zero-field susceptibility but with an exponent that is too small by a factor of two. Therefore, the Gutzwiller approach also underestimates the value of the zero-field spin susceptibility, see Fig. 12.

D. Spin correlation function

1. Local moment

In Fig. 13 we show the local moment on the impurity site, $C_{dd} = \langle (n_{d,\uparrow} - n_{d,\downarrow})^2 \rangle / 4$ from Gutzwiller, Hartree-Fock, and DMRG. The Gutzwiller approach provides a reasonable estimate for the local moment for all interaction strengths. However, it underestimates its value for weak interactions and slightly overestimates it in the strong-coupling limit.

Hartree-Fock theory uses the non-interacting Fermi-sea ground state for weak interactions, and starts with the interaction-driven build-up of the local moment at $U_c^{\text{HF}} \approx \pi\Gamma$. Similarly to the Hartree-Fock energy curve

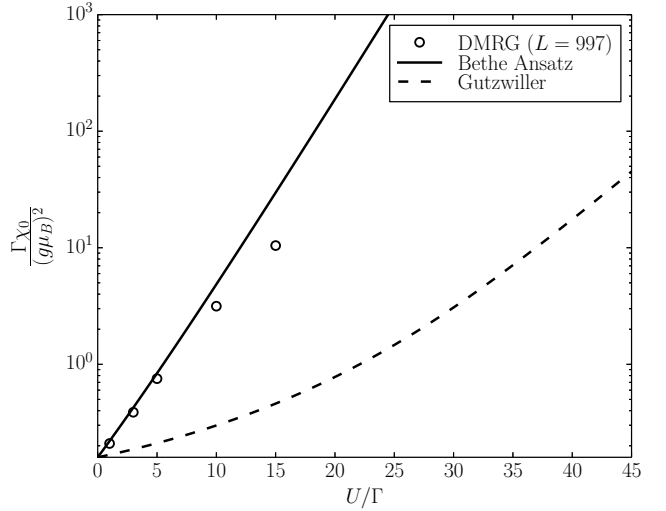


FIG. 12. (Color online) Zero-field magnetic susceptibility, $\Gamma\chi_0/(g\mu_B)^2$, as a function of the interaction strength $u = U/\Gamma$ from Bethe Ansatz, eq. (119), and the Gutzwiller variational approach, eq. (84), for the SIAM, in comparison with DMRG results for $L = 997$ sites. Note the logarithmic scale for the ordinate.

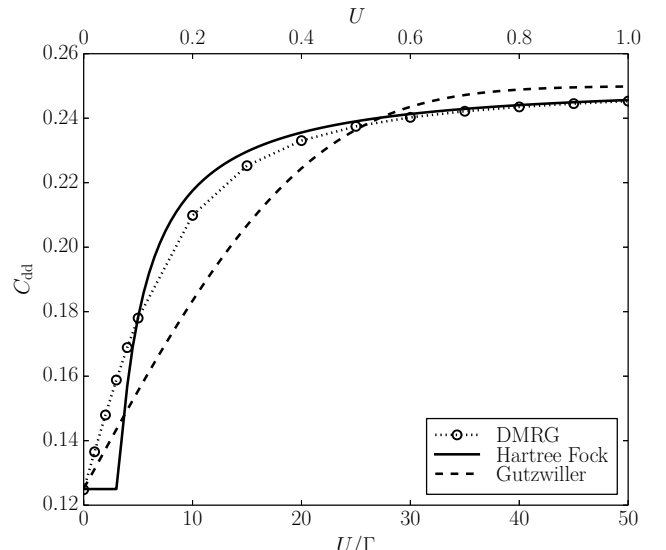


FIG. 13. Local spin correlation $C_{dd} = \langle (n_{d,\uparrow} - n_{d,\downarrow})^2 \rangle / 4$ for $V = 0.1$ ($\Gamma = 2V^2 = 0.02$) as a function of $U/\Gamma = 5$ in Gutzwiller and Hartree-Fock theory for the SIAM compared with DMRG results with $L = 1397$ sites.

shown in Fig. 8, a kink in $C_{dd}^{\text{HF}}(U)$ is observed at the critical Hartree-Fock interaction. For moderate to strong interactions, $U \gtrsim 5\Gamma$, it provides an excellent estimate for the local spin correlation. For $U/\Gamma = 5$ and for $U/\Gamma = 50$, the magnitude of the local moment is of the same magnitude both in the Gutzwiller approach and in Hartree-Fock theory.

2. Unscreened spin

In Fig. 14 we show the unscreened spin $\mathcal{S}(r)$ for $U/\Gamma = 5$ (upper panel) and $U/\Gamma = 50$ (lower panel) at $V = 0.1$ ($\Gamma = 0.02$). Even for $U/\Gamma = 5$, the asymptotic region is not yet reached for $L = 797$ in DMRG where by construction the spin is screened at $r = (L-1)/2 = 398$. For $U/\Gamma = 5$, finite-size effects are unimportant up to $r \approx 30$. When the interaction is very large, $U = 50\Gamma$, finite-size effects dominate the DMRG data for all $r > 1$.

Despite its failure to describe the ground-state energy properly, the Gutzwiller approach reproduces the mesoscopically large Kondo screening cloud. For $r \rightarrow \infty$, the impurity spin is perfectly screened, $\mathcal{S}^G(r \rightarrow \infty) = 0$, but the Kondo cloud extends over many thousands of sites even for moderately strong interactions, $U/\Gamma = 5$. In contrast, in magnetic Hartree-Fock theory the screening is never complete, $\mathcal{S}^{\text{HF}}(r \rightarrow \infty) > 0$. Therefore, among the three approaches discussed here, the Gutzwiller wave functions provides the best *qualitative* description of the Kondo screening cloud for strong couplings.

3. Fermi liquid regime

The calculation of the static spin correlation function $C_{dc}(r)$ in eq. (41) poses a difficult many-body problem. We separate the spin correlation function into its Fermi-liquid contribution (dressed bubble) and a part that contains vertex parts in a diagrammatic approach,

$$C_{dc}^S(r) = C_{dc}^{S,\text{FL}} + C_{dc}^{S,x},$$

$$C_{dc}^{S,\text{FL}} = -\frac{1}{2} \left| \langle \Psi_0 | \hat{c}_{r,\uparrow}^\dagger \hat{d}_{\uparrow} | \Psi_0 \rangle \right|^2 = -\frac{1}{2} M_r^2. \quad (120)$$

The vertex part vanishes for the non-interacting case, see eq. (63). For the Fermi-liquid part, we used that the d -electron density is one half and that the system is unpolarized.

Due to particle-hole symmetry for the translational invariant system, the Fermi-liquid contribution vanishes for odd sites, $C_{dc}^{S,\text{FL}}(2m+1) = 0$. The spin correlation function at odd sites remain small even for substantial interactions. However, from the DMRG data we infer that, for large interactions and intermediate length scales, the vertex term for even sites is (much) larger than the Fermi-liquid contribution. In this regime, the ground state is very far from a single Slater determinant.

In the limit of very large distances and thus small excitation energies, we expect that the Fermi liquid picture description is applicable. For the Fermi liquid contribution we can write quite generally²⁵

$$M_{2m} = -\frac{V}{\pi} \int_{-\pi/2}^0 dp \text{Im} \left[[\sin(2mp) - i \cos(2mp)] \tilde{G}_{d,d}^{\text{ret}}(\sin(p)/2) \right], \quad (121)$$

where we neglected the contributions from the bound states because their contribution vanishes exponentially

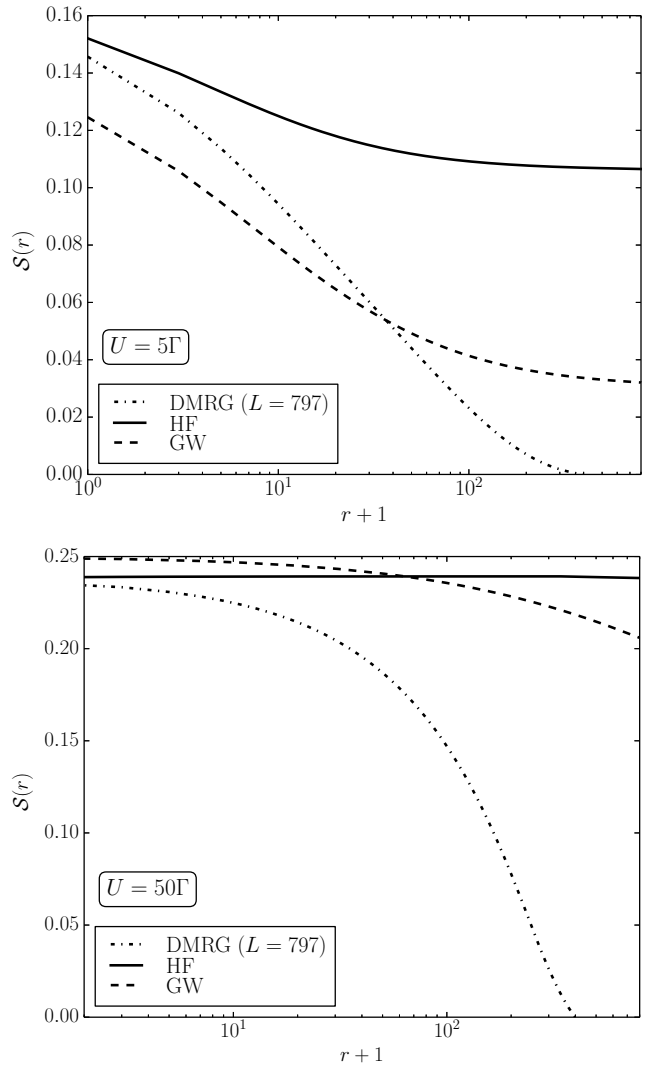


FIG. 14. Unscreened spin $\mathcal{S}(r)$ at distance r from the impurity site, see eq. (43), for $V = 0.1$ ($\Gamma = 2V^2 = 0.02$), $U/\Gamma = 5$ (upper panel) and $U/\Gamma = 50$ (lower panel). The Gutzwiller and magnetic Hartree-Fock results for the SIAM are compared with DMRG results with $L = 797$ sites.

for large distances. Here, $\tilde{G}_{d,d}^{\text{ret}}(\omega)$ is the exact retarded impurity Green function.

At very large distances, only the region of small p contributes to the integration because of the vastly oscillating sine and cosine functions. Thus, we may approximate the impurity spectral function by its Fermi-liquid form,

$$D_{d,d}(\omega) \approx \frac{1}{\pi} \frac{\Gamma_*}{\omega^2 + \Gamma_*^2} \quad (122)$$

with $\Gamma_* \propto T_L$ with the Kondo scale from eq. (104). Thus, we recover the result (70) for the decay of the spin correlation function at large distances, $m \gg 1/(4\Gamma_*)$,

$$C_{dc}^S(2m \gg 1/(2\Gamma_*^2)) \approx -\frac{V^2}{8\pi^2\Gamma_*^2} \frac{1}{m^2}. \quad (123)$$

The long-range decay of the correlation function is algebraic but, since Γ_* is exponentially small, this decay only sets in at exponentially large length scales. The Gutzwiller approach reproduces this result qualitatively.

VI. CONCLUSIONS

In this work, we studied the ground-state energy, the impurity magnetization and susceptibility, and the Kondo screening cloud for the symmetric single-impurity Anderson model (SIAM) using the results from the Gutzwiller, magnetic Hartree-Fock, and DMRG variational approaches. For the ground-state energy and magnetic properties, we compared our results to those from the Bethe Ansatz that become exact in the wide-band limit. For further reference, we defer many technical details to the supplemental material.²⁵

Each of the three variational methods has its merits and limitations.

– The Hartree-Fock approach provides an excellent description of the ground-state energy for intermediate to strong couplings. However, since it displays a gap for (magnetic) excitations, Hartree-Fock theory fails to reproduce the large magnetic susceptibility for strong couplings. Concomitantly, it is unable to screen the impurity spin.

The Hartree-Fock theory correctly describes the charge excitations of the symmetric SIAM. This makes it the perfect starting point for more elaborate analytical approximations such as the local-moment approach that introduces the missing low-energy spin-flip processes into the Hartree-Fock description.^{10–12}

– Gutzwiller theory provides a rather poor upper bound for the ground-state energy. However, it qualitatively describes the exponentially large magnetic zero-field susceptibility for strong couplings because it retains an exponentially small resonance in the impurity density of states in the Kondo limit. Consequently, the impurity spin is completely screened by the bath electrons at infinite distance from the impurity.

As an inherent Fermi-liquid description, Gutzwiller theory correctly reproduces the long-range behavior of the Kondo cloud. However, for short and intermediate distances, its description of the Kondo cloud is too simple-minded.

– The DMRG method is numerically essentially exact for finite systems. In this work, we map the SIAM on a ring onto a two-chain geometry with open boundary conditions where we may disregard the inter-chain coupling for large system sizes. Therefore, we can treat rings with up to $L = 1400$ sites, and extrapolations of the ground-state energy to

the thermodynamic limit are unproblematic. We see that the Bethe Ansatz description is applicable for interactions up to about half the bandwidth even at $V = 0.1W$.

The intrinsic energy resolution is limited to $\Delta\omega = W/L$. Therefore, the DMRG encounters problems to resolve the Abrikosov-Suhl resonance in the impurity density of states in the strong-coupling limit, and a reliable description of the impurity magnetization and of the magnetic susceptibility is limited to moderate interaction strengths. Correspondingly, DMRG properly describes the short-range region of the Kondo cloud but does not cover the long-distance asymptotics because the Kondo cloud in DMRG cannot exceed half the system size.

At the end of our presentation, we emphasize that the Kondo screening cloud is amazingly large, even in the non-interacting limit and in one dimension where a larger fraction of the bath electrons can couple to the impurity than in higher dimensions. This implies that magnetic impurities in metals can be correlated over mesoscopic distances.

Note, however, that this behavior depends on a number of assumptions, namely, (i), a perfect metallic host without impurities, (ii), exact particle-hole and spin-flip symmetry, and, (iii), zero temperature. Deviations from these exceptional conditions, especially a finite temperature, will drastically limit the range over which the impurity spin is screened.

Nevertheless, we can expect that two magnetic impurities in a metal can sense each others' presence over quite some distance so that they will bind into magnetic singlet (or triplet) pairs. An investigation of this pairing requires the analysis of the two-impurity Anderson model (TIAM), see, e.g., Ref. [39] for a recent Gutzwiller variational study, and references therein. A DMRG study of the TIAM is currently under way.

ACKNOWLEDGMENTS

This research has been supported in part by the Hungarian National Research, Development and Innovation Office (NKFIH) through Grant No. K120569 and PD-17-125261 and the Hungarian Quantum Technology National Excellence Program (Project No. 2017-1.2.1-NKP-2017-00001).

Appendix A: Equation-of-motion approach

1. Causal and retarded Green functions

The causal Green function for the fermionic Heisenberg operators $\hat{A}(t) = \exp(i\hat{H}_0 t)\hat{A} \exp(-i\hat{H}_0 t)$ and \hat{B}^+

is defined by

$$\begin{aligned} G_{A,B}^c(t) &= (-i)\hat{T}\langle\hat{A}(t)\hat{B}^+\rangle \\ &= (-i)\Theta(t)\langle\hat{A}(t)\hat{B}^+\rangle + i\Theta(-t)\langle\hat{B}^+\hat{A}(t)\rangle. \end{aligned} \quad (\text{A1})$$

Equal-time expectation values $\langle\hat{B}^+\hat{A}\rangle$ in the ground state $|0\rangle \equiv |\Phi_0\rangle$ can be directly calculated from the causal Green functions by taking the limit $t \rightarrow 0^-$.

For the equation-of-motion approach, it is more convenient to study the retarded Green function,

$$G_{A,B}^{\text{ret}}(t) = (-i)\Theta(t)\langle[\hat{A}(t), \hat{B}^+]\rangle_+. \quad (\text{A2})$$

Its Fourier transformation is defined by

$$\begin{aligned} \tilde{G}_{A,B}^{\text{ret}}(\omega) &= \int_0^\infty dt e^{(i\omega-\eta)t} G_{A,B}^{\text{ret}}(t) \\ &= \int_{-\infty}^\infty d\omega' \frac{D_{A,B}(\omega')}{\omega - \omega' + i\eta}. \end{aligned} \quad (\text{A3})$$

Here, the density of states is defined by

$$\begin{aligned} D_{A,B}(\omega) &= \sum_m \left[\langle 0|\hat{B}^+|m\rangle\langle m|\hat{A}|0\rangle \delta(\omega - E_0 + E_m) \right. \\ &\quad \left. + \langle 0|\hat{A}|m\rangle\langle m|\hat{B}^+|0\rangle \delta(\omega + E_0 - E_m) \right], \end{aligned} \quad (\text{A4})$$

where $|m\rangle$ denotes the eigenstates of \hat{H}_0 with energy E_m (Lehmann representation). Using the Lehmann representation it is readily shown that

$$\tilde{G}_{a,b}^c(\omega) = \int_{-\infty}^\infty d\omega' \frac{D_{A,B}(\omega')}{\omega - \omega' + i\eta \text{sgn}(\omega)} \quad (\text{A5})$$

with the sign function $\text{sgn}(x) = |x|/x$. Therefore, the causal Green function is obtained from the retarded Green function by replacing $\omega + i\eta$ by $\omega + i\eta \text{sgn}(\omega)$.

When $\hat{A} \neq \hat{B}$, the density of states $D_{A,B}(\omega)$ is not necessarily real. We separate the real and imaginary part,

$$D_{A,B}(\omega) = \frac{D_{A,B}(\omega) + D_{A,B}^*(\omega)}{2} + i\frac{D_{A,B}(\omega) - D_{A,B}^*(\omega)}{2i} \quad (\text{A6})$$

and use $D_{A,B}^*(\omega) = D_{B,A}(\omega)$ to find

$$\begin{aligned} D_{A,B}(\omega) &= -\frac{1}{\pi} \text{Im} \left[\frac{G_{A,B}^{\text{ret}}(\omega) + G_{B,A}^{\text{ret}}(\omega)}{2} \right] \\ &\quad - \frac{i}{\pi} \text{Im} \left[\frac{G_{A,B}^{\text{ret}}(\omega) - G_{B,A}^{\text{ret}}(\omega)}{2i} \right]. \end{aligned} \quad (\text{A7})$$

For $\hat{A} = \hat{B}$ we recover the standard expression

$$D_{A,A}(\omega) = -\frac{1}{\pi} \text{Im} [G_{A,A}^{\text{ret}}(\omega)]. \quad (\text{A8})$$

2. Green functions for the non-interacting SIAM

a. Time domain

For the non-interacting symmetric SIAM, we study the four retarded Green functions

$$G_{k,p;\sigma}^{\text{ret}}(t) = (-i)\Theta(t)\langle[\hat{c}_{k,\sigma}(t), \hat{c}_{p,\sigma}^+]\rangle_+, \quad (\text{A9})$$

$$G_{d,p;\sigma}^{\text{ret}}(t) = (-i)\Theta(t)\langle[\hat{d}_{\sigma}(t), \hat{c}_{p,\sigma}^+]\rangle_+, \quad (\text{A10})$$

$$G_{k,d;\sigma}^{\text{ret}}(t) = (-i)\Theta(t)\langle[\hat{c}_{k,\sigma}(t), \hat{d}_{\sigma}^+]\rangle_+, \quad (\text{A11})$$

$$G_{d,d;\sigma}^{\text{ret}}(t) = (-i)\Theta(t)\langle[\hat{d}_{\sigma}(t), \hat{d}_{\sigma}^+]\rangle_+, \quad (\text{A12})$$

Taking the time derivative leads to

$$\begin{aligned} i\dot{G}_{k,p;\sigma}^{\text{ret}}(t) &= \delta(t)\delta_{k,p} + (-i)\Theta(t)\langle[\hat{c}_{k,\sigma}(t), \hat{H}_0]_-, \hat{c}_{p,\sigma}^+\rangle_+ \\ &= \delta(t)\delta_{k,p} + \epsilon(k)G_{k,p;\sigma}^{\text{ret}}(t) + \frac{V_k^*}{\sqrt{L}}G_{d,p;\sigma}^{\text{ret}}(t), \end{aligned} \quad (\text{A13})$$

$$\begin{aligned} i\dot{G}_{d,p;\sigma}^{\text{ret}}(t) &= (-i)\Theta(t)\langle[\hat{d}_{\sigma}(t), \hat{H}_0]_-, \hat{c}_{p,\sigma}^+\rangle_+ \\ &= \sum_k \frac{V_k}{\sqrt{L}}G_{k,p;\sigma}^{\text{ret}}(t) - E_{d,\sigma}G_{d,p;\sigma}^{\text{ret}}(t), \end{aligned} \quad (\text{A14})$$

$$\begin{aligned} i\dot{G}_{k,d;\sigma}^{\text{ret}}(t) &= (-i)\Theta(t)\langle[\hat{c}_{k,\sigma}(t), \hat{H}_0]_-, \hat{d}_{\sigma}^+\rangle_+ \\ &= \epsilon(k)G_{k,d;\sigma}^{\text{ret}}(t) + \frac{V_k^*}{\sqrt{L}}G_{d,d;\sigma}^{\text{ret}}(t), \end{aligned} \quad (\text{A15})$$

$$\begin{aligned} i\dot{G}_{d,d;\sigma}^{\text{ret}}(t) &= \delta(t) + (-i)\Theta(t)\langle[\hat{d}_{\sigma}(t), \hat{H}_0]_-, \hat{d}_{\sigma}^+\rangle_+ \\ &= \delta(t) + \sum_k \frac{V_k}{\sqrt{L}}G_{k,d;\sigma}^{\text{ret}}(t) - E_{d,\sigma}G_{d,d;\sigma}^{\text{ret}}(t). \end{aligned} \quad (\text{A16})$$

Here, we used the anticommutation relations of the Fermi operators and the commutation relations

$$\begin{aligned} [\hat{c}_{k,\sigma}, \hat{T}]_- &= \epsilon(k)\hat{c}_{k,\sigma}, [\hat{d}_{\sigma}, \hat{T}]_- = 0, \\ [\hat{c}_{k,\sigma}, \hat{V}]_- &= \frac{V_k^*}{\sqrt{L}}\hat{d}_{\sigma}, [\hat{d}_{\sigma}, \hat{V}]_- = \sum_k \frac{V_k}{\sqrt{L}}\hat{c}_{k,\sigma}, \\ [\hat{d}_{\sigma}, \hat{P}]_- &= -E_{d,\sigma}\hat{d}_{\sigma}. \end{aligned} \quad (\text{A17})$$

In the presence of an external magnetic field for the bath electrons, $\epsilon(k)$ must be replaced by $\epsilon(k) - \sigma_n B_{\text{bath}}$ with $\sigma_n = 1$ ($\sigma_n = -1$) for $\sigma = \uparrow$ ($\sigma = \downarrow$). For non-interacting electrons, the equations of motion lead to a closed set of differential equations (A13)–(A16).

b. Explicit solution in the frequency domain

The equation-of-motion method works in the frequency domain. The Fourier transformation of the time deriva-

tive of retarded Green functions are given by

$$\begin{aligned} \text{FT} \left\{ i\dot{G}_{A,B}^{\text{ret}}(t) \right\} (\omega) &= \int_{-\infty}^{\infty} dt e^{-\eta|t|} e^{i\omega t} \left(i\dot{G}_{A,B}^{\text{ret}}(t) \right) \\ &= i \left[G_{A,B}^{\text{ret}}(t) e^{-\eta|t|} e^{i\omega t} \right]_{-\infty}^{\infty} \\ &\quad - \int_0^{\infty} dt G_{A,B}^{\text{ret}}(t) \frac{d}{dt} (e^{-\eta t} e^{i\omega t}) \\ &= (\omega + i\eta) \tilde{G}_{A,B}^{\text{ret}}(\omega), \end{aligned} \quad (\text{A18})$$

where we used partial integration in the first step and the fact that $G_{A,B}^{\text{ret}}(t < 0) = 0$.

To solve the equations (A13)–(A16) we transform them into frequency space. We find

$$(\omega + E_{d,\sigma} + i\eta) \tilde{G}_{d,d;\sigma}^{\text{ret}}(\omega) = 1 + \sum_k \frac{V_k}{\sqrt{L}} \tilde{G}_{k,d;\sigma}^{\text{ret}}(\omega), \quad (\text{A19})$$

$$(\omega + E_{d,\sigma} + i\eta) \tilde{G}_{d,p;\sigma}^{\text{ret}}(\omega) = \sum_k \frac{V_k}{\sqrt{L}} \tilde{G}_{k,p;\sigma}^{\text{ret}}(\omega), \quad (\text{A20})$$

$$(\omega - \epsilon(k) + i\eta) \tilde{G}_{k,d;\sigma}^{\text{ret}}(\omega) = \frac{V_k^*}{\sqrt{L}} \tilde{G}_{d,d;\sigma}^{\text{ret}}(\omega), \quad (\text{A21})$$

$$(\omega - \epsilon(k) + i\eta) \tilde{G}_{k,p;\sigma}^{\text{ret}}(\omega) = \delta_{k,p} + \frac{V_k^*}{\sqrt{L}} \tilde{G}_{d,p;\sigma}^{\text{ret}}(\omega). \quad (\text{A22})$$

The resulting set of equations is readily solved. We define the retarded hybridization function

$$\Delta^{\text{ret}}(\omega) = \frac{1}{L} \sum_k \frac{|V_k|^2}{\omega - \epsilon(k) + i\eta}, \quad (\text{A23})$$

and find

$$\tilde{G}_{d,d;\sigma}^{\text{ret}}(\omega) = \frac{1}{\omega + E_{d,\sigma} - \Delta^{\text{ret}}(\omega)}, \quad (\text{A24})$$

$$\tilde{G}_{k,d;\sigma}^{\text{ret}}(\omega) = \sqrt{\frac{1}{L}} \frac{V_k^*}{(\omega - \epsilon(k) + i\eta)(\omega + E_{d,\sigma} - \Delta^{\text{ret}}(\omega))}, \quad (\text{A25})$$

$$\tilde{G}_{d,p;\sigma}^{\text{ret}}(\omega) = \sqrt{\frac{1}{L}} \frac{V_p}{(\omega - \epsilon(p) + i\eta)(\omega + E_{d,\sigma} - \Delta^{\text{ret}}(\omega))}, \quad (\text{A26})$$

and

$$\begin{aligned} \tilde{G}_{k,p;\sigma}^{\text{ret}}(\omega) &= \frac{1}{\omega - \epsilon(k) + i\eta} \left(\delta_{k,p} \right. \\ &\quad \left. + \frac{1}{L} \frac{V_p V_k^*}{(\omega - \epsilon(p) + i\eta)(\omega + E_{d,\sigma} - \Delta^{\text{ret}}(\omega))} \right). \end{aligned} \quad (\text{A27})$$

The equations for the causal Green functions are obtained by replacing η by $\eta \text{sgn}(\omega)$. In the presence of a magnetic field for the bath electrons, we must replace $\Delta^{\text{ret}}(\omega)$ by $\Delta_{\sigma}^{\text{ret}}(\omega) = \Delta(\omega + \sigma_n B_{\text{bath}})$.

Appendix B: Spectral properties

To simplify the analysis, we shall consider the case $V_k = V > 0$. Moreover, we study the case of a one-dimensional ring with electron transfers between nearest-neighbors and bandwidth $W \equiv 1$,

$$\epsilon(k) = -\cos(k)/2 \quad \text{for } |k| \leq \pi. \quad (\text{B1})$$

The non-interacting density of states becomes

$$\rho_0(\epsilon) = \frac{2}{\pi\sqrt{1-4\epsilon^2}} \quad \text{for } |\epsilon| \leq 1/2 \quad (\text{B2})$$

so that $d_0 = \rho_0(0) = 2/\pi$ for the density of states in one dimension.

1. Impurity spectral function

First, we work out the impurity spectral function from the impurity Green function (A24). We have

$$\begin{aligned} \Delta^{\text{ret}}(\omega) &= V^2 \int_{-1/2}^{1/2} d\epsilon \frac{\rho_0(\epsilon)}{\omega - \epsilon + i\eta} \\ &= V^2 \Lambda_0(\omega) - i\pi V^2 \rho_0(\omega). \end{aligned} \quad (\text{B3})$$

In one dimension, $\Lambda_0(\omega) = 0$ for $|\omega| \leq 1/2$ and

$$\Lambda_0(\omega) = \frac{2\text{sgn}(\omega)}{\sqrt{4\omega^2 - 1}} \quad (\text{B4})$$

for $|\omega| > 1/2$. Thus, we have

$$\begin{aligned} \omega + E_{d,\sigma} - \Delta^{\text{ret}}(\omega) &= \omega + E_{d,\sigma} + i\pi V^2 \rho_0(\omega) \\ &\quad (|\omega| \leq 1/2), \\ &= \omega + E_{d,\sigma} - \frac{2V^2 \text{sgn}(\omega)}{\sqrt{4\omega^2 - 1}} + i\eta \\ &\quad (|\omega| > 1/2). \end{aligned} \quad (\text{B5})$$

We keep the infinitesimal imaginary part $\eta = 0^+$ because of the (anti-)bound states outside the host-electron band.

The density of states for the d -electrons (' d -electron spectral function') follows from eq. (A4) as

$$\begin{aligned} D_{d,d;\sigma}(\omega) &= -\frac{1}{\pi} \text{Im} \left(\frac{1}{\omega + E_{d,\sigma} - \Delta_{\sigma}^{\text{ret}}(\omega)} \right) \\ &= \frac{V^2 \rho_0(\omega_{\sigma})}{(\pi \rho_0(\omega_{\sigma}) V^2)^2 + (\omega + E_{d,\sigma})^2} \quad \text{for } |\omega_{\sigma}| \leq 1/2 \end{aligned} \quad (\text{B6})$$

with $\omega_{\sigma} = \omega + \sigma_n B_{\text{bath}}$. For $|\omega_{\sigma}| > 1/2$ we have

$$\begin{aligned} D_{d,d;\sigma}(\omega) &= \delta \left(\omega + E_{d,\sigma} + \frac{2V^2}{\sqrt{4\omega_{\sigma}^2 - 1}} \right) \\ &\quad + \delta \left(\omega + E_{d,\sigma} - \frac{2V^2}{\sqrt{4\omega_{\sigma}^2 - 1}} \right). \end{aligned} \quad (\text{B7})$$

For $B_{\text{bath}} = E_{d,\sigma} = 0$, we can further write

$$D_{d,d;\sigma}(\omega) = Z(V)\delta\left(\omega + \frac{v_+}{2}\right) + Z(V)\delta\left(\omega - \frac{v_+}{2}\right) \quad (\text{B8})$$

with

$$\begin{aligned} Z(V) &= \left[\frac{\partial}{\partial\omega} (\omega - \Delta^{\text{ret}}(\omega))_{\pm v_+/2} \right]^{-1} \\ &= \frac{1}{1 + 4V^2 v_+/v_-^3}, \\ v_{\pm}(V) &= \frac{\sqrt{\sqrt{1+64V^4} \pm 1}}{\sqrt{2}} \equiv v_{\pm}. \end{aligned} \quad (\text{B9})$$

The bound and anti-bound states at $\omega = \pm v_+/2$ contribute two poles of strength $Z(V)$ to the impurity spectral function. For small V , we have $v_+/2 \approx 1/2 + 4V^4$, $v_-/2 \approx 2V^2$, and $Z(V) \approx 16V^4$. The pole contributions are very small for small V , of order V^4 .

For $E_{d,\sigma} \neq 0$, it is best to determine the energies of (anti-)bound state $v_b(V, E_{d\sigma}) < -1/2$ [$v_{ab}(V, E_{d\sigma} > 1/2)$], and their strengths $Z_b(V)$ [$Z_{ab}(V)$] numerically from the equations

$$P_{\pm}(v_{b/\text{ab}}) = 0, \quad Z_{b/\text{ab}}(V) = [P'_{\pm}(v_{b/\text{ab}})]^{-1}, \quad (\text{B10})$$

where

$$P_{\pm}(\omega) = \omega + E_{d,\sigma} \pm \frac{2V^2}{\sqrt{4\omega_{\sigma}^2 - 1}}. \quad (\text{B11})$$

2. Density of states

The single-particle density of states is defined by

$$D_{\sigma}(\omega) = \sum_m \delta(\omega - E_m). \quad (\text{B12})$$

To make contact with the retarded Green functions, we write the single-particle density of states in the form

$$\begin{aligned} D_{\sigma}(\omega) &= -\frac{1}{\pi} \text{Im} \left(\sum_m \langle \hat{a}_{m,\sigma}^+ \frac{1}{\omega - (\hat{H}_0 - E_0) + i\eta} \hat{a}_{m,\sigma} \rangle \right. \\ &\quad \left. + \langle \hat{a}_{m,\sigma} \frac{1}{\omega - (\hat{H}_0 - E_0) + i\eta} \hat{a}_{m,\sigma}^+ \rangle \right), \end{aligned} \quad (\text{B13})$$

where we used the fact that $\hat{a}_{m,\sigma}^+$ ($\hat{a}_{m,\sigma}$) creates (annihilates) an electron with exact single-particle energy E_m in the ground state. The sum over m runs over all single-particle excitations of the ground state and thus represents the trace over all single-particle eigenstates,

$$D_{\sigma}(\omega) = -\frac{1}{\pi} \text{Im} \text{Tr}_1 \left(\frac{1}{\omega - (\hat{H}_0 - E_0) + i\eta} \right). \quad (\text{B14})$$

We can equally use the excitations $\hat{c}_{k,\sigma}^+ |\Phi_0\rangle$, $\hat{c}_{k,\sigma} |\Phi_0\rangle$, and $\hat{d}_{\sigma}^+ |\Phi_0\rangle$, $\hat{d}_{\sigma} |\Phi_0\rangle$, respectively, to perform the trace

over the single-particle excitations of the ground state. Therefore, we may write

$$\begin{aligned} D_{\sigma}(\omega) &= -\frac{1}{\pi} \text{Im} \left[\sum_k \left(\langle \hat{c}_{k,\sigma}^+ \frac{1}{\omega - (\hat{H}_0 - E_0) + i\eta} \hat{c}_{k,\sigma} \right. \right. \\ &\quad \left. \left. + \langle \hat{c}_{k,\sigma} \frac{1}{\omega - (\hat{H}_0 - E_0) + i\eta} \hat{c}_{k,\sigma}^+ \rangle \right) \right. \\ &\quad \left. + \langle \hat{d}_{\sigma}^+ \frac{1}{\omega - (\hat{H}_0 - E_0) + i\eta} \hat{d}_{\sigma} \rangle \right. \\ &\quad \left. + \langle \hat{d}_{\sigma} \frac{1}{\omega - (\hat{H}_0 - E_0) + i\eta} \hat{d}_{\sigma}^+ \rangle \right] \\ &= -\frac{1}{\pi} \text{Im} \left[\sum_k G_{k,k}^{\text{ret}}(\omega) + G_{d,d}^{\text{ret}}(\omega) \right]. \end{aligned} \quad (\text{B15})$$

Equation (A27) shows that the band Green function consists of the undisturbed host Green function for $V_k \equiv 0$ and a $1/L$ correction due to the hybridization. Therefore, using eqs. (A24) and (A27), the contribution due to a finite hybridization is given by

$$\begin{aligned} D_{\text{imp},\sigma}(\omega) &= -\frac{1}{\pi} \text{Im} \left[\frac{1}{\omega + E_{d,\sigma} - \Delta^{\text{ret}}(\omega)} \right. \\ &\quad \left. \times \left(1 + \sum_k \frac{|V_k|^2/L}{(\omega - \epsilon(k) + i\eta)^2} \right) \right] \\ &= -\frac{1}{\pi} \text{Im} \left[\frac{1 - (\partial\Delta^{\text{ret}}(\omega))/(\partial\omega)}{\omega + E_{d,\sigma} - \Delta^{\text{ret}}(\omega)} \right] \\ &= -\frac{1}{\pi} \frac{\partial}{\partial\omega} \text{Im} [\ln(\omega + E_{d,\sigma} - \Delta^{\text{ret}}(\omega))]. \end{aligned} \quad (\text{B16})$$

We find the band contribution for $|\omega| < 1/2$ from the complex logarithm

$$D_{\text{imp},\sigma}^{\text{band}}(\omega) = -\frac{1}{\pi} \frac{\partial}{\partial\omega} \left[\text{Cot}^{-1} \left(\frac{\omega + E_{d,\sigma} - V^2 \Lambda_0(\omega)}{\pi \rho_0(\omega) V^2} \right) \right], \quad (\text{B17})$$

where $\text{Cot}^{-1}(x) = \pi\Theta(-x) + \cot^{-1}(x)$ is continuous and differentiable across $x = 0$; $\Theta(x)$ is the Heaviside step function. We shall use this form for the calculation of the ground-state energy, see below.

Using eq. (B5) and (B11), the (anti-)bound states contribute

$$\begin{aligned} D_{\text{imp},\sigma}^{\text{b/ab}}(\omega) &= -\frac{1}{\pi} \frac{\partial}{\partial\omega} \left[\text{Cot}^{-1} \left(\frac{\eta}{P_{\pm}(\omega)} \right) \right] \\ &= \frac{1}{\pi} \frac{\eta P'_{\pm}(\omega)}{P_{\pm}^2(\omega) + \eta^2}. \end{aligned} \quad (\text{B18})$$

When we let $\eta \rightarrow 0$, we only retain a contribution where $P_{\pm}(\omega) = 0$, i.e., at $\omega_{\pm} = v_{b/\text{ab}}(V, E_{d\sigma})$. Thus,

$$\begin{aligned} D_{\text{imp},\sigma}^{\text{b/ab}}(\omega) &= \frac{1}{\pi} \frac{\eta Z_{b/\text{ab}}(V)}{(\omega - v_{b/\text{ab}})^2 + (Z_{b/\text{ab}}(V)\eta)^2} \\ &= \delta(\omega - v_b(V, E_{d\sigma})) + \delta(\omega - v_{ab}(V, E_{d\sigma})), \end{aligned} \quad (\text{B19})$$

where we let $\eta \rightarrow 0^+$ in the last step. We see that the (anti-)bound states contribute poles of strength unity to

the density of states in the presence of the impurity. Recall that their contribution to the impurity spectral function was smaller by the weight factor $Z_{a/b}(V) \ll 1$.

Appendix C: Ground-state expectation values

In this section we derive the ground-state expectation values for the energy, the d -occupancy, and the hybridization matrix element for the symmetric SIAM.

1. Ground-state energy

a. Symmetric SIAM

We consider the case $E_{d,\sigma} = 0$. The ground-state energy can immediately be calculated using the density of states. We subtract the energy for $V = 0$ and write

$$e_0(V) = 2 \int_{-\infty}^0 d\omega \omega D_{\text{imp},\sigma}(\omega) = e_0^b(V) + e_0^{\text{band}}(V). \quad (\text{C1})$$

The upper limit of integration is zero because all single-particle states up to the Fermi energy $E_F = 0$ are occupied.

Using eq. (B19), the contribution from the bound state is given by

$$e_0^b(V) = 2 \left(\frac{1}{2} - \frac{v_+}{2} \right) = 1 - v_+, \quad (\text{C2})$$

where we measure the energy contribution with respect to the lower band edge, $\epsilon_{\text{edge}} = -1/2$. For small V , the contribution is very small, $e_0^b(V \ll 1) \approx -8V^4$.

The result for the band contribution to the impurity density of states (B17) and a partial integration lead to the band contribution to the ground-state energy in the form

$$\begin{aligned} e_0^{\text{band}}(V) &= R(V) + \frac{2}{\pi} \int_{-1/2}^0 d\omega \cot^{-1} \left(\frac{\omega - V^2 \Lambda_0(\omega)}{\pi \rho_0(\omega) V^2} \right), \\ R(V) &= -1 - \frac{2}{\pi} \left[\omega \text{Cot}^{-1} \left(\frac{\omega - V^2 \Lambda_0(\omega)}{\pi \rho_0(\omega) V^2} \right) \right]_{-1/2-\eta}^0 \\ &\quad + \frac{2}{\pi} \int_{-1/2}^0 d\omega \pi \Theta \left(-\frac{\omega - V^2 \Lambda_0(\omega)}{\pi \rho_0(\omega) V^2} \right). \end{aligned} \quad (\text{C3})$$

The first term in $R(V)$ accounts for the energy term introduced in the definition (C2) of the bound-state energy. It is compensated by the last term in $R(V)$. The second term gives a zero contribution at $\omega = 0$ because $\text{Cot}^{-1}(0)$ is finite. It is more subtle to evaluate the second term at $\omega = -1/2$ because, in one dimension, neither $\Lambda_0(\omega)$ nor $\rho_0(\omega)$ are continuous. This problem is circumvented by using a finite $\bar{\eta}$ in eq. (B3). For $\bar{\eta} > 0$ we thus see that $\Lambda_0(-1/2 - \eta) \rightarrow -\infty$, $\rho_0(-1/2 - \eta) \rightarrow 0^+$ so that we encounter $\text{Cot}^{-1}(+\infty) = 0$ so that the second term vanishes altogether. Therefore, we find $R(V) = 0$.

In one dimension, using $\Lambda_0(\omega) = 0$ and $\rho_0(\omega)$ for $|\omega| < 1/2$ from eq. (B2), MATHEMATICA⁴⁰ gives the band contribution

$$\begin{aligned} e_0^{\text{band}}(V) &= \frac{2}{\pi} \int_{-1/2}^0 d\epsilon \cot^{-1} \left(\frac{\epsilon \sqrt{1 - 4\epsilon^2}}{2V^2} \right) \\ &= \frac{1}{2\pi} \left[-\pi + 2v_+ \arctan \left(\frac{1}{v_-} \right) \right. \\ &\quad \left. + v_- \ln \left(\frac{v_+ - 1}{v_+ + 1} \right) \right]. \end{aligned} \quad (\text{C4})$$

The total energy reads

$$\begin{aligned} e_0(V) &= \frac{1}{2\pi} \left[-\pi + 2v_+ \arctan \left(\frac{1}{v_-} \right) \right. \\ &\quad \left. + v_- \ln \left(\frac{v_+ - 1}{v_+ + 1} \right) \right] + (1 - v_+). \end{aligned} \quad (\text{C5})$$

b. Limit of small hybridization

For $V \ll 1$ we Taylor expand $e_0(V)$ in eq. (C5),

$$e_0^{\text{small}}(V) = \frac{4V^2}{\pi} (\ln(V^2) + \ln(2) - 1) - 4V^4. \quad (\text{C6})$$

Corrections are of the order $V^6 \ln(V^2)$. For $V = 0.1$, the approximate formula works very well. We have $E_{\text{SIAM}}^{(0)}(V)(0.1) = -0.06291$ whereas the approximation gives $E_{\text{SIAM}}^{\text{small}}(0.1) = -0.06294$, with a relative error of less than one per mill.

The result agrees with the small- V expression derived as eqs. (E.1) and (E.5) by Linneweber and collaborators.³⁹ Using MATHEMATICA⁴⁰ we find in one dimension using $d_0 = \rho_0(0) = 2/\pi$ and $\ln(e) = 1$

$$C = \frac{e}{2} \exp \left(\int_{-1/2}^0 d\epsilon \frac{d_0 - \rho_0(\epsilon)}{d_0 \epsilon} \right) = e \quad (\text{C7})$$

so that, up to corrections of the order V^4 ,

$$\begin{aligned} e_0^{\text{small}}(V) &= 2V^2 d_0 \ln \left(\frac{\pi V^2 d_0}{C} \right) \\ &= \frac{4V^2}{\pi} (\ln(V^2) + \ln(2) - 1). \end{aligned} \quad (\text{C8})$$

2. Expectation values from Green functions

The Green functions permit the calculation of ground-state expectation values. By definition, we have ($\eta = 0^+$)

$$\begin{aligned} \langle \hat{B}^+ \hat{A} \rangle &= (-i) G_{A,B}^c(t = -\eta) = \int_{-\infty}^{\infty} \frac{d\omega}{2\pi i} e^{i\eta\omega} \tilde{G}_{A,B}^c(\omega) \\ &= \int_{-\infty}^{\infty} d\omega' D_{A,B}(\omega') \int_{-\infty}^{\infty} \frac{d\omega}{2\pi i} \frac{e^{i\eta\omega}}{\omega - \omega' + i\eta' \text{sgn}(\omega')} \\ &= \int_{-\infty}^0 d\omega' D_{A,B}(\omega'), \end{aligned} \quad (\text{C9})$$

where we used eq. (A5) in the second step. In the last step we extended the ω -integral to a contour integral in the upper complex plane that includes the real axis and an arc around the origin with infinite radius. The residue theorem then results in $\Theta(-\omega')$ because a pole of strength unity appears in the upper complex plane only for $\text{sgn}(\omega') = -1$.

For the d -electron occupancy, we set $\hat{A} = \hat{B} = \hat{d}_\sigma$ and find from eqs. (A8), (B6), and (B7)

$$\langle \hat{d}_\sigma^+ \hat{d}_\sigma \rangle = Z(V) + \int_{-1/2}^0 d\omega \frac{\rho_0(\omega) V^2}{\omega^2 + (\pi \rho_0(\omega) V^2)^2}. \quad (\text{C10})$$

Apparently, this expression is symmetric in ω so that one readily recovers $\langle \hat{d}_\sigma^+ \hat{d}_\sigma \rangle = 1/2$.

3. Hybridization

a. General expression

The derivation of the hybridization matrix element proceeds along the same lines. As in the previous subsection C 2 we find

$$M(\epsilon(k)) \equiv \sqrt{L} \langle \hat{c}_{k,\sigma}^+ \hat{d}_\sigma \rangle = \sqrt{L} \int_{-\infty}^0 d\omega D_{k,d}(\omega). \quad (\text{C11})$$

Using eqs. (A4), (A25), and (A26) we find

$$D_{k,d}(\omega) = -\frac{1}{\pi} \frac{V}{\sqrt{L}} \text{Im} \left[\frac{1}{(\omega - \epsilon(k) + i\eta)(\omega - \Delta^{\text{ret}}(\omega))} \right] \quad (\text{C12})$$

because $G_{k,d;\sigma}^{\text{ret}}(\omega) = G_{d,k;\sigma}^{\text{ret}}(\omega)$ for real hybridizations V_k . Particle-hole symmetry gives $M(\epsilon) = M^*(-\epsilon) = M(-\epsilon)$ because $M(\epsilon)$ is real.

For the hybridization matrix element in position space we thus find

$$\begin{aligned} M_r &= \int_0^\pi \frac{dk}{\pi} \cos(kr) M(\epsilon(k)) \\ &= (1 + (-1)^r) \int_0^{\pi/2} \frac{dk}{\pi} \cos(kr) M(\epsilon(k)) \end{aligned} \quad (\text{C13})$$

so that M_r is zero on for odd distances, $r = 2m + 1$. For $\omega \leq 0$ we use

$$\begin{aligned} Q_r(\omega) &= \int_0^\pi \frac{dk}{\pi} \frac{\cos(kr)}{\omega - \epsilon(k) + i\eta} \\ &= (-i) i^r \int_0^\infty dt e^{i\omega t} J_r(t/2) \\ &= -\frac{2}{\sqrt{4\omega^2 - 1}} \left(\sqrt{4\omega^2 - 1} - 2\omega \right)^{-r} \\ &\quad \text{for } \omega < -1/2, \\ &= -\frac{(2i) i^r}{\cos(p)} [\cos(pr) + i \sin(pr)] \\ &\quad \text{for } -1/2 < \omega = \sin(p)/2 \leq 0 \end{aligned} \quad (\text{C14})$$

to find two contributions for M_r . First, the pole at energy $\omega = -v_+/2 < -1/2$ in $D_{k,d}(\omega)$ gives the bound-state contribution

$$\begin{aligned} M_r^b &= V Z(V) Q_r(-v_+/2) \\ &= -\frac{2V Z(V)}{\sqrt{v_+^2 - 1}} \left(\sqrt{v_+^2 - 1} + v_+ \right)^{-r}. \end{aligned} \quad (\text{C15})$$

The bound-state contribution to M_r is of the order V^3 for small V and becomes exponentially small for $r \gg 1/(4V^2)$. Second, the band contribution can be cast into the form

$$\begin{aligned} M_{2m}^{\text{band}} &= -\frac{2V(-1)^m}{\pi} \int_0^\pi du \frac{\cos(u/2)}{\sin^2 u + 64V^4} \\ &\quad \times [\sin(u) \cos(mu) + 8V^2 \sin(mu)]. \end{aligned} \quad (\text{C16})$$

Its limiting behavior is discussed in the main text.

b. Matrix element in momentum space

It is instructive to study the matrix element $M(\epsilon)$ in more detail. Since we are interested in the small- V limit, we ignore the bound-state contribution and focus on the band contribution for $\epsilon > 0$ so that $1/(\omega - \epsilon)$ remains finite,

$$H(\epsilon) = \int_{-1/2}^0 d\omega \frac{1}{\omega - \epsilon} \frac{\rho_0(\omega) V^2}{\omega^2 + (\pi V^2 \rho_0(\omega))^2}. \quad (\text{C17})$$

Note, however, that the integrand develops a singularity for $\epsilon \rightarrow 0^+$. We treat the singularity $1/(\omega - \epsilon)$ explicitly and write

$$\begin{aligned} H(\epsilon) &= H_1(\epsilon) + \int_{-1/2}^0 \frac{d\omega}{\omega - \epsilon} (f_V(\omega) - f_V(\epsilon)), \\ H_1(\epsilon) &= f_V(\epsilon) \int_{-1/2}^0 \frac{d\omega}{\omega - \epsilon} = f_V(\epsilon) \ln \left| \frac{\epsilon}{\epsilon + 1/2} \right| \end{aligned} \quad (\text{C18})$$

with

$$f_V(\epsilon) = \frac{2V^2}{\pi} \frac{\sqrt{1 - 4\epsilon^2}}{4V^4 + \epsilon^2(1 - 4\epsilon^2)}. \quad (\text{C19})$$

We define

$$g_V(\epsilon) = \frac{2V^2}{\pi} \frac{1 - 4\epsilon^2}{4V^4 + \epsilon^2(1 - 4\epsilon^2)} \quad (\text{C20})$$

and write

$$\begin{aligned} H(\epsilon) &= H_1(\epsilon) + H_2(\epsilon) + H_3(\epsilon), \\ H_2(\epsilon) &= \int_{-1/2}^0 \frac{d\omega}{\omega - \epsilon} (g_V(\omega) - g_V(\epsilon)), \end{aligned} \quad (\text{C21})$$

$$\begin{aligned} H_3(\epsilon) &= \int_{-1/2}^0 \frac{d\omega}{\omega - \epsilon} (f_V(\omega) - g_V(\omega) - f_V(\epsilon) + g_V(\epsilon)). \end{aligned} \quad (\text{C22})$$

The term $H_2(\epsilon)$ can be cast into the form

$$H_2(\epsilon) = -\frac{2V^2}{\pi} \frac{1}{4V^4 + \epsilon^2(1 - 4\epsilon^2)} \times \int_{-1/2}^0 d\omega(\epsilon + \omega) \frac{16V^4 + (1 - 4\omega^2)(1 - 4\epsilon^2)}{4V^4 + \omega^2(1 - 4\omega^2)}. \quad (\text{C23})$$

We thus have

$$H_2(\epsilon) = -\frac{2V^2}{\pi} \frac{1 - 4\epsilon^2}{4V^4 + \epsilon^2(1 - 4\epsilon^2)} [\epsilon \Lambda_1(V) + \Lambda_2(V)] - \frac{2V^2}{\pi} \frac{1}{4V^4 + \epsilon^2(1 - 4\epsilon^2)} [\epsilon \Lambda_3(V) + \Lambda_4(V)]. \quad (\text{C24})$$

MATHEMATICA⁴⁰ provides closed formulae for $\Lambda_{1-4}(V)$,

$$\begin{aligned} \Lambda_1(V) &= \frac{v_+^3 \arctan(1/v_-)}{2V^2 \sqrt{1 + 64V^4}} - \frac{v_-^3 \operatorname{arctanh}(1/v_+)}{2V^2 \sqrt{1 + 64V^4}}, \\ \Lambda_2(V) &= \frac{\ln[(1 + 32V^4 - \sqrt{1 + 64V^4})/(32V^4)]}{2\sqrt{1 + 64V^4}}, \\ \Lambda_3(V) &= \frac{8V^2(v_+ \arctan(1/v_-) + v_- \operatorname{arctanh}(1/v_+))}{\sqrt{1 + 64V^4}}, \\ \Lambda_4(V) &= \frac{16V^4 \ln[(1 + 32V^4 - \sqrt{1 + 64V^4})/(32V^4)]}{\sqrt{1 + 64V^4}}. \end{aligned} \quad (\text{C25})$$

Lastly, we set $V = 0$ in the integrand of $H_3(\epsilon)$ after taking out the factor $\epsilon^2(1 - 4\epsilon^2)/(4V^4 + \epsilon^2(1 - 4\epsilon^2))$. Note that the integrand in eq. (C22) is well behaved for $\omega \rightarrow 0$, $\epsilon \rightarrow 0$, and $\omega \rightarrow \epsilon$ so that corrections are indeed small, of the order $V^4 \ln(V^2)$, V^4 ,

$$H_3(\epsilon) \approx \frac{2V^2\epsilon^2(1 - 4\epsilon^2)}{\pi(4V^4 + \epsilon^2(1 - 4\epsilon^2))} \times \int_{-1/2}^0 \frac{d\omega}{\omega - \epsilon} \left[\frac{(1 - \sqrt{1 - 4\omega^2})}{\omega^2 \sqrt{1 - 4\omega^2}} - \frac{(1 - \sqrt{1 - 4\epsilon^2})}{\epsilon^2 \sqrt{1 - 4\epsilon^2}} \right]. \quad (\text{C26})$$

The integral can be done using MATHEMATICA.⁴⁰ We find

$$H_3(\epsilon) \approx \frac{2V^2\sqrt{1 - 4\epsilon^2}}{\pi(4V^4 + \epsilon^2(1 - 4\epsilon^2))} \times \left[(\ln(2) - 2\epsilon)\sqrt{1 - 4\epsilon^2} + \ln\left(\frac{1 + 2\epsilon}{1 + \sqrt{1 - 4\epsilon^2}}\right) \right]. \quad (\text{C27})$$

The analytical approximation to $H(\epsilon)$ is thus given by

$$H(\epsilon) = H_1(\epsilon) + H_2(\epsilon) + H_3(\epsilon) \quad (\text{C28})$$

with corrections of the order $V^4 \ln(V^2)/(4V^4 + \epsilon^2(1 - 4\epsilon^2))$.

We may perform the small- V expansion for $H(\epsilon)$. To leading order we have

$$\begin{aligned} \Lambda_1(V \ll 1) &= \frac{\pi}{4V^2} - 2 - 2\pi V^2 + \mathcal{O}(V^4 \ln(V^2)), \\ \Lambda_2(V \ll 1) &= \ln(4V^2) + \mathcal{O}(V^4 \ln(V^2)), \\ \Lambda_3(V \ll 1) &= 4\pi V^2 + \mathcal{O}(V^4 \ln(V^2)), \\ \Lambda_4(V \ll 1) &= \mathcal{O}(V^4 \ln(V^2)). \end{aligned} \quad (\text{C29})$$

Consequently, the leading contribution to $H_2(\epsilon)$ is given by

$$H_2(\epsilon) = -\frac{1}{2} \frac{\epsilon(1 - 4\epsilon^2)}{4V^4 + \epsilon^2(1 - 4\epsilon^2)} + \frac{4V^2\epsilon(1 - 4\epsilon^2)}{\pi(4V^4 + \epsilon^2(1 - 4\epsilon^2))} - \frac{2V^2 \ln(4V^2)(1 - 4\epsilon^2)}{\pi(4V^4 + \epsilon^2(1 - 4\epsilon^2))} + \mathcal{O}(V^4). \quad (\text{C30})$$

Therefore, the small- V expansion for all $-1/2 \leq \epsilon \leq 1/2$ becomes

$$\begin{aligned} H(\epsilon) &\approx -\frac{1}{2} \frac{|\epsilon|(1 - 4\epsilon^2)}{4V^4 + \epsilon^2(1 - 4\epsilon^2)} \\ &+ \frac{2V^2}{\pi} \frac{\sqrt{1 - 4\epsilon^2}}{4V^4 + \epsilon^2(1 - 4\epsilon^2)} \\ &\times \left[-\ln(2V^2) \sqrt{1 - 4\epsilon^2} + \ln\left(\frac{2\epsilon}{1 + \sqrt{1 - 4\epsilon^2}}\right) \right]. \end{aligned} \quad (\text{C31})$$

Corrections are of the order $V^4 \ln(V^2)/(4V^4 + \epsilon^2(1 - 4\epsilon^2))$. As required by particle-hole symmetry, $H(-\epsilon) = H(\epsilon)$.

For small- V and low energies, $\epsilon \rightarrow 0$, the result can be cast into

$$\begin{aligned} H(\epsilon \rightarrow 0^+, V \rightarrow 0) &\approx H^{\text{low}}(\epsilon), \\ H^{\text{low}}(\epsilon) &= -\frac{1}{2} \frac{\epsilon}{4V^4 + \epsilon^2} + \frac{2V^2 \ln[\epsilon/(2V^2)]}{\pi 4V^4 + \epsilon^2}. \end{aligned} \quad (\text{C32})$$

This form is sufficient to determine the long-range behavior of the spin correlation function for small V .

Appendix D: Further results for the non-interacting SIAM

In this section we collect some results for the semi-elliptic density of states, consider the limit of small hybridizations for a general density of states, and provide results for non-interacting electrons in the limit of high dimensions.

1. Semi-elliptic density of states

For the semi-elliptic density of states,

$$\rho_0(\epsilon) = \frac{4}{\pi} \sqrt{1 - 4\epsilon^2} \quad \text{for } |\epsilon| \leq 1/2, \quad (\text{D1})$$

we find

$$\begin{aligned}\Lambda_0(\omega) &= 8\omega \quad \text{for } |\omega| \leq 1/2, \\ &= 8\omega - 4\text{sgn}(\omega)\sqrt{4\omega^2 - 1} \quad \text{for } |\omega| > 1/2.\end{aligned}\quad (\text{D2})$$

When we choose $0 \leq V < 1/4$, there is no (anti-)bound state outside the band.

a. Ground-state energy

The ground-state energy can be calculated analytically using MATHEMATICA⁴⁰,

$$\begin{aligned}e_0(V) &= \frac{2}{\pi} \int_{-1/2}^0 d\omega \cot^{-1} \left(\frac{\omega - V^2 \Lambda_0(\omega)}{\pi \rho_0(\omega) V^2} \right) \\ &= -\frac{4V^2}{\pi \sqrt{1 - 16V^2}} \ln \left[\frac{1 - 8V^2 + \sqrt{1 - 16V^2}}{1 - 8V^2 - \sqrt{1 - 16V^2}} \right].\end{aligned}\quad (\text{D3})$$

The result agrees with the small- V expression derived as eqs. (E.1) and (E.5) in Ref. [39]. Using MATHEMATICA⁴⁰ we find for the semi-elliptic density of states using $d_0 = \rho_0(0) = 4/\pi$ and $\ln(e) = 1$

$$C = \frac{e}{2} \exp \left(\int_{-1/2}^0 d\epsilon \frac{d_0 - \rho_0(\epsilon)}{d_0 \epsilon} \right) = 1 \quad (\text{D4})$$

so that, up to corrections of the order $V^4 \ln(V^2)$,

$$e_0^{\text{small}}(V) = 2V^2 d_0 \ln \left(\frac{\pi V^2 d_0}{C} \right) = \frac{8V^2}{\pi} \ln(4V^2). \quad (\text{D5})$$

b. Hybridization matrix element

For the semi-elliptic density of states, the hybridization function can be calculated analytically. For $0 < V < 1/4$ and $0 < \epsilon < 1/2$ we find

$$\begin{aligned}H(\epsilon) &= \int_{-1/2}^0 d\omega \frac{1}{\omega - \epsilon} \frac{\rho_0(\omega) V^2}{[\omega(1 - 8V^2)]^2 + (\pi \rho_0(\omega) V^2)^2} \\ &= \frac{4V^2}{\pi} \int_{-1/2}^0 d\omega \frac{1}{\omega - \epsilon} \frac{\sqrt{1 - 4\omega^2}}{16V^4 + \omega^2(1 - 16V^2)} \\ &= -\frac{1}{2} \frac{\epsilon(1 - 8V^2)}{16V^4 + (1 - 16V^2)\epsilon^2} \\ &\quad + \frac{4V^2(1 - 8V^2)}{\pi \sqrt{1 - 16V^2}} \frac{\text{arccsch}(8V^2/\sqrt{1 - 16V^2})}{16V^4 + (1 - 16V^2)\epsilon^2} \\ &\quad - \frac{4V^2\sqrt{1 - 4\epsilon^2}}{\pi(16V^4 + (1 - 16V^2)\epsilon^2)} \ln \left(\frac{1}{2\epsilon} + \sqrt{\frac{1}{4\epsilon^2} - 1} \right),\end{aligned}\quad (\text{D6})$$

where $\text{arccsch}(x)$ is the inverse hyperbolic cosecant function.

The small- V expansion reads

$$\begin{aligned}H(\epsilon) &\approx -\frac{1}{2} \frac{\epsilon}{16V^4 + (1 - 16V^2)\epsilon^2} \\ &\quad + \frac{4V^2}{\pi(16V^4 + (1 - 16V^2)\epsilon^2)} \\ &\quad \times \left[\pi\epsilon + \sqrt{1 - 4\epsilon^2} \ln \left(\frac{2\epsilon}{1 + \sqrt{1 - 4\epsilon^2}} \right) \right. \\ &\quad \left. - \ln(4V^2) - 8V^2 \right].\end{aligned}\quad (\text{D7})$$

Corrections to this expression are of the order $V^6 \ln(V^2)/(16V^4 + (1 - 16V^2)\epsilon^2)$. The low-energy limit of this expression becomes

$$\begin{aligned}H(\epsilon \rightarrow 0^+, V \rightarrow 0) &\approx H^{\text{low}}(\epsilon), \\ H^{\text{low}}(\epsilon) &= -\frac{1}{2} \frac{\epsilon}{16V^4 + \epsilon^2} + \frac{4V^2 \ln[\epsilon/(4V^2)]}{\pi 16V^4 + \epsilon^2},\end{aligned}\quad (\text{D8})$$

compare eq. (C32) for the one-dimensional density of states.

2. Limit of small hybridizations for a general density of states

Here, we collect results for any density of states in the in finite band-width limit where we approximate $\rho(\epsilon) \approx d_0$ and $\Lambda_0(\epsilon) \approx 0$. Thus, $\Delta^{\text{ret}}(\omega) \approx -i\pi d_0 V^2$.

a. Ground-state energy

For the ground-state energy we obtain

$$\begin{aligned}e_0(V) &= \frac{2}{\pi} \int_{-1/2}^0 d\omega \cot^{-1} \left(\frac{\omega - V^2 \Lambda_0(\omega)}{\pi \rho_0(\omega) V^2} \right) \\ &\approx 2d_0 V^2 \ln \left[\frac{2\pi d_0 V^2}{C} \right],\end{aligned}\quad (\text{D9})$$

where C is used to fit the unknown contribution to order V^2 . In general,

$$C = \frac{e}{2} \exp \left(\int_{-1/2}^0 d\epsilon \frac{d_0 - \rho_0(\epsilon)}{d_0 \epsilon} \right) \quad (\text{D10})$$

for a given density of states $\rho_0(\epsilon)$.³⁹

b. Hybridization matrix element

For $H(\epsilon)$ we obtain

$$\begin{aligned}H(\epsilon) &\approx \int_{-1/2}^0 d\omega \frac{1}{\omega - \epsilon} \frac{d_0 V^2}{\omega^2 + (\pi d_0 V^2)^2} \\ &= \frac{-2\epsilon \text{arccot}(2\gamma) + \gamma \ln[(1 + 4\gamma^2)\epsilon^2 / (\gamma^2(1 + 2\epsilon)^2)]}{2\pi(\gamma^2 + \epsilon^2)}\end{aligned}\quad (\text{D11})$$

with $\gamma = \pi d_0 V^2$ and $\text{arccot}(x)$ denotes the inverse cotangent function.

The low-energy limit for small V becomes

$$H(\epsilon \rightarrow 0^+, V \rightarrow 0) \approx H^{\text{low}}(\epsilon),$$

$$H^{\text{low}}(\epsilon) = -\frac{1}{2} \frac{\epsilon}{(\pi d_0 V^2)^2 + \epsilon^2} + d_0 V^2 \frac{\ln[\epsilon/(\pi d_0 V^2)]}{(\pi d_0 V^2)^2 + \epsilon^2}. \quad (\text{D12})$$

The results includes eq. (C32) for the one-dimensional density of states ($d_0 = 2/\pi$) and eq. (D8) for the semi-elliptic density of states ($d_0 = 4/\pi$). Therefore, eq. (D12) provides the generic low-energy limit of the function $H(\epsilon)$.

3. Limit of high dimensions

We address the limit of high dimensions. To this end we focus on a d -dimensional hyper-cubic lattice with nearest-neighbor dispersion relation [$\mathbf{k} = (k_1, k_2, \dots, k_d)$]

$$\epsilon(\mathbf{k}) = -\frac{2}{\sqrt{2d}} \sum_{l=1}^d \cos(k_l). \quad (\text{D13})$$

We restrict ourselves to the case of half band-filling and particle-hole symmetry.

a. Bulk spin correlation function

The spin-spin correlation function for free electrons is obtained from

$$C^{SS}(r) = \frac{1}{L} \sum_{\mathbf{l}} \langle \hat{S}^z(\mathbf{l} + \mathbf{r}) \hat{S}^z(\mathbf{l}) \rangle \quad (\text{D14})$$

$$= -\frac{1}{2} \frac{1}{L} \sum_{\mathbf{l}} \left| \langle \hat{c}_{\mathbf{l}+\mathbf{r},\sigma}^+ \hat{c}_{\mathbf{l},\sigma} \rangle \right|^2 = -\frac{1}{2} |P_{\sigma}^0(\mathbf{r})|^2$$

with the single-particle density matrix

$$P_{\sigma}^0(\mathbf{r}) = \langle \hat{c}_{\mathbf{l}+\mathbf{r},\sigma}^+ \hat{c}_{\mathbf{l},\sigma} \rangle$$

$$= \frac{1}{L} \sum_{\mathbf{k}} e^{-i\mathbf{kr}} \langle \hat{c}_{\mathbf{k},\sigma}^+ \hat{c}_{\mathbf{k},\sigma} \rangle$$

$$= \int_{-\infty}^0 d\epsilon \int_{-\infty}^{\infty} \frac{d\eta}{2\pi} e^{i\eta\epsilon} \prod_{l=1}^d \int_{-\pi}^{\pi} \frac{dk}{2\pi} e^{2in\cos(k)/\sqrt{2d} - ikr_l}$$

$$= \int_{-\infty}^0 d\epsilon \int_{-\infty}^{\infty} \frac{d\eta}{2\pi} e^{i\eta\epsilon} \prod_{l=1}^d i^{r_l} J_{r_l}(2\eta/\sqrt{2d}), \quad (\text{D15})$$

where $J_n(x) = (-1)^n J_n(x)$ is the Bessel function of integer order n . We introduce the distance to the R th neighbor shell,

$$R = \sum_{l=1}^d |r_l| \quad (\text{D16})$$

and use $d \gg 1$ to approximate

$$\prod_{l=1}^d J_{r_l}(2\eta/\sqrt{2d}) \approx e^{-\eta^2/2} \left(\frac{\eta}{\sqrt{2d}} \right)^R \prod_{l=1}^d (r_l!)^{-1}, \quad (\text{D17})$$

where we used $J_0(x \ll 1) \approx 1 - x^2/4$ and $J_{n \geq 1}(x \ll 1) \approx (x/2)^n/n!$. Therefore,

$$P_{\sigma}^0(\mathbf{r}) \approx \left(\frac{i}{\sqrt{2d}} \right)^R \prod_l \frac{1}{r_l!} \int_{-\infty}^0 d\epsilon \int_{-\infty}^{\infty} \frac{d\eta}{2\pi} e^{i\eta\epsilon} \eta^R e^{-\eta^2/2}. \quad (\text{D18})$$

When $R = 2m$ is even, we find $P_{\sigma}^0(\mathbf{r}) = \delta_{m,0}/2$, as also follows from particle-hole symmetry.

When $R = 2m+1$ ($m \geq 0$) we note that the dominant contribution in the R th neighbor shell comes from those vectors where $r_l = \pm 1$. Their number is given by

$$N(d, R) = 2^R \binom{d}{R} \approx (2d)^R \frac{1}{R!} \quad (\text{D19})$$

for $d \gg R$ where we used Stirling's formula, $\ln(n!) \approx n \ln n - n$.

We write

$$P_{\sigma}^0(\mathbf{r}) \approx P_{\sigma}^0(R),$$

$$P_{\sigma}^0(R) = \left(\frac{1}{\sqrt{2d}} \right)^R \int_{-\infty}^0 \frac{d\epsilon}{\sqrt{2\pi}} \left(\frac{\partial}{\partial \epsilon} \right)^R \left[e^{-\epsilon^2/2} \right]$$

$$= \left(\frac{1}{\sqrt{2d}} \right)^R \frac{(-1)^{R-1}}{\sqrt{2\pi}} \text{He}_{R-1}(0)$$

$$= \left(\frac{1}{\sqrt{2d}} \right)^R \frac{1}{\sqrt{2\pi}} \left(-\frac{1}{2} \right)^{(R-1)/2} \frac{(R-1)!}{((R-1)/2)!}, \quad (\text{D20})$$

where $\text{He}(x)$ is a Hermite polynomial. The contribution of the R th neighbor shell to the spin-spin correlation function ($R = 2m+1$) is

$$C^{SS}(R) = -\frac{1}{2} \sum_{|\mathbf{r}|=R} |P_{\sigma}^0(\mathbf{r})|^2$$

$$\approx -\frac{1}{2} \frac{1}{(2m+1)!} \frac{1}{2\pi} \left(\frac{1}{2} \right)^{2m} \left(\frac{(2m)!}{m!} \right)^2$$

$$= -\frac{1}{4\pi} \frac{1}{2m+1} \left(\frac{1}{2} \right)^{2m} \binom{2m}{m}. \quad (\text{D21})$$

This approximation becomes exact in the limit $d \rightarrow \infty$.

For large R we use Stirling's formula, $\ln(n!) \approx n \ln n - n + \ln(2\pi n)/2$, to find the asymptotic behavior (R odd)

$$C^{SS}(R \gg 1) \approx - \left(\frac{1}{2\pi R} \right)^{3/2}. \quad (\text{D22})$$

b. Spin correlation function

Along the same lines we can express the matrix element for the spin correlation function between the impurity

and the host electrons at distance $R = 2m$ as

$$M_R = \frac{2V}{\sqrt{2\pi}} 2^{-R/2} \left(\frac{-1}{\sqrt{2d}} \right)^R \int_0^\infty d\epsilon H(\epsilon) e^{-\epsilon^2/2} H_R(\epsilon/\sqrt{2}), \quad (\text{D23})$$

where $H_R(x)$ is a Hermite polynomial. As in one dimension, correlations to odd sites vanish due to particle-hole symmetry.

Averaged over all sites at distance $R \ll d$, the spin correlation function becomes ($\Gamma = \pi d_0 V^2$, $\Gamma = \sqrt{\pi/2} V^2$ for an infinite-dimensional hyper-cubic lattice)

$$C_{dc}^S(R) = -\frac{1}{2} \left(\frac{2V}{\sqrt{2\pi}} \right)^2 [g(R, \Gamma)]^2, \\ g(R, \Gamma) = \frac{2^{-R/2}}{\sqrt{R!}} \int_0^\infty dy \tilde{H}(y) e^{-\Gamma^2 y^2/2} H_R(\Gamma y/\sqrt{2}), \quad (\text{D24})$$

where we used eq. (D19) for the number of sites in the R th neighbor shell. Moreover, for small V we may use the low-energy limit of $H(\epsilon)$,

$$\tilde{H}(y) \approx -\frac{1}{2} \frac{y}{1+y^2} + \frac{1}{\pi} \frac{\ln(y)}{1+y^2}. \quad (\text{D25})$$

To derive an asymptotic formula, we employ the approximation

$$H_{R \gg 1}(x) \approx e^{x^2/2} (-2)^{R/2} (R-1)!! \cos(\sqrt{2R}x) \quad (\text{D26})$$

for $R \gg 1$ and $|x| < \sqrt{2R}$. Since the integral contains another factor $\exp(-x^2/2)$, we may safely ignore the constraint on x . Thus, for small hybridizations, $V \ll 1$, we may approximate

$$|g(R, \Gamma)| \approx \frac{(R-1)!!}{\sqrt{R!}} \int_0^\infty dy \tilde{H}(y) e^{-\Gamma^2 y^2/4} \cos(\Gamma \sqrt{R}y). \quad (\text{D27})$$

For $\Gamma \ll 1$ we may safely ignore the exponential term in the definition of $g(R, \Gamma)$ because the cosine is a vastly oscillating function for $y \gtrsim 1/\Gamma$ that effectively restricts the integration to $y \lesssim 1/(\Gamma \sqrt{R})$. Then, the integral can be done analytically,

$$g(R, \Gamma) \approx (-1)^{R/2} \frac{(R-1)!!}{\sqrt{R!}} \left[\frac{1}{2} e^{\Gamma \sqrt{R}} \text{Ei}(-\Gamma \sqrt{R}) \right], \quad (\text{D28})$$

where $\text{Ei}(x)$ is the exponential integral. As in one dimension, the approximation works very well for all $R \geq 2$. Using Stirling's formula $\ln(n!) \approx n \ln n - n + \ln(2\pi n)/2$, we find ($R = 2m$)

$$\frac{((R-1)!!)^2}{R!} = \frac{(2m)!(2m)!}{2^{2m} m! m!(2m)!} \approx \sqrt{\frac{2}{\pi R}}. \quad (\text{D29})$$

Consequently, the spin correlation function becomes

$$C_{dc}^S(R) \approx -\frac{1}{2} \left(\frac{2V}{\sqrt{2\pi}} \right)^2 \sqrt{\frac{2}{\pi R}} \left[\frac{1}{2} e^{\Gamma \sqrt{R}} \text{Ei}(-\Gamma \sqrt{R}) \right]^2. \quad (\text{D30})$$

The formula is applicable for all $R \geq 2$.

The asymptotic region is reached for $\Gamma \sqrt{R} \gg 1$, i.e., for $R \gg 1/\Gamma^2 = 2/(\pi V^4)$. Even for $V = 0.1$, the asymptotic region starts around $R_a = \mathcal{O}(V^4) = 10^4$, in contrast to the one-dimensional case where the asymptotic region starts at $R_a = \mathcal{O}(V^2) = 10^2$. In the asymptotic regime,

$$C_{dc}^S(R \gg 1/\Gamma^2) \approx -\frac{1}{2\pi^2 \Gamma} \left(\frac{1}{R} \right)^{3/2}, \quad (\text{D31})$$

so that the unscreened spin is given by

$$S(R \gg 1/\Gamma^2) = \frac{1}{2\pi^2 \Gamma \sqrt{R}}. \quad (\text{D32})$$

In $d \rightarrow \infty$ dimensions, the unscreened spin decays proportional to $1/\sqrt{R}$ whereas, in $d = 1$ dimension, it decays proportional to $1/R$.

Appendix E: Interacting SIAM

In this section, we address the interacting single-impurity Anderson model. First, we calculate the second-order coefficient in U for the ground-state energy. Next, we derive the ground-state energy for the magnetic Hartree-Fock solution.

1. Second-order coefficient for the ground-state energy

a. Brückner-Goldstone perturbation theory

Using Brückner-Goldstone perturbation theory,⁴¹ the second-order coefficient reads⁴²

$$-\frac{e^{(2)}(V)}{\pi \Gamma} = \langle \Phi_0 | \hat{H}_{\text{int}} \frac{1}{E_0(V) - \hat{H}_0} \hat{H}_{\text{int}} | \Phi_0 \rangle, \quad (\text{E1})$$

where we used the definition of $e^{(2)}(V)$ in the main text and $\hat{H}_{\text{int}} = (\hat{n}_{d,\uparrow} - 1/2)(\hat{n}_{d,\downarrow} - 1/2)$. Since we subtracted the Hartree terms in \hat{H}_{int} , we only sum over connected diagrams in eq. (E1). With $\eta = 0^+$ we can write

$$-\frac{e^{(2)}(V)}{\pi \Gamma} = \text{Re} \left[(-i) \int_0^\infty dt e^{-\eta t} \langle \Phi_0 | \hat{H}_{\text{int}} e^{i(E_0(V) - \hat{H}_0)t} \hat{H}_{\text{int}} | \Phi_0 \rangle \right] \\ = \int_0^\infty dt e^{-\eta t} \text{Im} [f(t)^2]. \quad (\text{E2})$$

Here, we introduced

$$f(t) = \langle (\hat{n}_{d,\sigma} - 1/2) e^{i(E_0(V) - \hat{H}_0)t} (\hat{n}_{d,\sigma} - 1/2) \rangle \\ = \langle \hat{d}_\sigma^+(t) \hat{d}_\sigma \rangle \langle \hat{d}_\sigma(t) \hat{d}_\sigma^+ \rangle, \quad (\text{E3})$$

where we used Wick's theorem. Particle-hole symmetry shows that the two factors are identical. Using the causal Green function for the d -electrons, we can write

$$f(t) = \Theta(t) [iG_{d,d}^c(t)]^2 \quad (\text{E4})$$

with

$$G_{d,d}^c(t \geq 0) = \int_{-\infty}^{\infty} \frac{d\omega}{2\pi} e^{-i\omega t} \tilde{G}_{d,d}^c(\omega). \quad (\text{E5})$$

We insert the spectral representation (A5) and extend the integral over ω into a contour integral in the lower complex half-plane because we have $t > 0$. The ω -integral gives $(-i)\Theta(\omega') \exp(-i\omega' t)$ because there is a pole in the lower complex half-plane only if $\omega' > 0$. Thus,

$$iG_{d,d}^c(t^+) = \int_0^{\infty} d\omega' e^{-i\omega' t} D_{d,d}(\omega'). \quad (\text{E6})$$

We insert this result into eq. (E2) and perform the integration to find

$$\begin{aligned} e^{(2)}(V) &= \pi \Gamma \int_0^{\infty} d\omega_1 D_{d,d}(\omega_1) \dots \int_0^{\infty} d\omega_4 D_{d,d}(\omega_4) \\ &\quad \times \frac{1}{\omega_1 + \omega_2 + \omega_3 + \omega_4} \\ &= \pi \int_0^{\infty} d\mu [F(V, \mu)]^4, \\ F(V, \mu) &= \int_0^{\infty} d\omega D_{d,d}(\omega) e^{-\mu\omega/\Gamma}. \end{aligned} \quad (\text{E7})$$

This form is numerically more advantageous than inserting eq. (E6) into eq. (E2) and taking the imaginary part. Using the Lehmann representation and the (symmetric) density of states for the d -electrons, one can obtain eq. (E7) from eq. (E1) directly.

For the one-dimensional density of states we have

$$\begin{aligned} F(V, \mu) &= Z(V) e^{-v+\mu/(2\Gamma)} \\ &\quad + \int_0^{1/(2\Gamma)} \frac{du}{\pi} e^{-u\mu} \frac{\sqrt{1-4u^2\Gamma^2}}{1+u^2(1-4u^2\Gamma^2)}. \end{aligned} \quad (\text{E8})$$

A numerical integration in eq. (E7) gives the coefficients $e^{(2)}(V = 0.05) = 0.0369271$, $e^{(2)}(V = 0.1) = 0.0374447$, and $e^{(2)}(V = 0.2) = 0.0406307$.

b. Limit of small hybridizations

In the limit of small hybridizations, we let $\Gamma \rightarrow 0$ and ignore the pole contribution of order V^4 . With $\Gamma = \pi d_0 V^2$ we find that $F(V, \mu)$ becomes independent of V , $F(V, \mu) \equiv F(\mu)$, with

$$F(\mu) = \frac{1}{\pi} \left(\text{Ci}(\mu) \sin(\mu) + \cos(\mu) \left(\frac{\pi}{2} - \text{Si}(\mu) \right) \right), \quad (\text{E9})$$

where $\text{Ci}(x)$ [$\text{Si}(x)$] is the cosine [sine] integral.

When we insert this result in eq. (E7), we obtain the numerical value $\tilde{e}^{(2)} = 0.0368608$, in perfect agreement with Yamada's analytical result,³⁵ $\tilde{e}^{(2)} = 1/4 - 7\zeta(3)/(4\pi^2)$, and in very good agreement with the numerically obtained value for $V \leq 0.2$. The deviations are about ten percent at $V = 0.2$, about one percent at $V = 0.1$, and two per mill at $V = 0.05$.

2. Magnetic Hartree-Fock solution

In the magnetic Hartree-Fock approach, the Hubbard interaction on the impurity is replaced by

$$H_{\text{int}}^{\text{HF}} = -Um(\hat{n}_{d,\uparrow} - 1/2) + Um(\hat{n}_{d,\downarrow} - 1/2) + Um^2, \quad (\text{E10})$$

$$m = \frac{\langle \hat{n}_{d,\uparrow} - \hat{n}_{d,\downarrow} \rangle}{2}. \quad (\text{E11})$$

Here, m is the local polarization of the impurity. To be definite, we restrict ourselves to $0 \leq m \leq 1/2$. Apparently, the Hartree-Fock Hamiltonian $\hat{H}^{\text{HF}} = \hat{H}_0 + H_{\text{int}}^{\text{HF}}$ corresponds to a non-interacting SIAM with spin-dependent local potentials, $E_{d,\uparrow} = Um$ and $E_{d,\downarrow} = -Um$.

a. Self-consistency equation

When we repeat the steps in Sect. C2 we arrive at

$$\begin{aligned} \langle \hat{n}_{d,\sigma} \rangle &= Z[v_b(V, \sigma_n Um)] \\ &\quad + \int_{-1/2}^0 d\omega \frac{\rho_0(\omega) V^2}{(\omega + \sigma_n Um)^2 + (\pi \rho_0(\omega) V^2)^2} \end{aligned} \quad (\text{E12})$$

with $\sigma_n = 1$ ($\sigma_n = -1$) for $\sigma = \uparrow$ ($\sigma = \downarrow$). Therefore, the self-consistency equation (E11) becomes

$$\begin{aligned} 2m &= Z[v_b(V, Um)] - Z[v_b(V, -Um)] \\ &\quad + \sum_{\sigma_n=\pm 1} \int_{-1/(2\Gamma)}^0 \frac{dx}{\pi} \frac{\sigma_n \rho_0(\Gamma x)/d_0}{(x + \sigma_n \tilde{u})^2 + (\rho_0(\Gamma x)/d_0)^2} \end{aligned} \quad (\text{E13})$$

with $\tilde{u} = Um/\Gamma$ ($\Gamma = \pi d_0 V^2$, $d_0 = \rho_0(0)$). For the one-dimensional density of states, the self-consistency equation explicitly reads

$$\begin{aligned} 2m &= Z[v_b(V, Um)] - Z[v_b(V, -Um)] \\ &\quad + \sum_{\sigma_n=\pm 1} \int_{-1/(2\Gamma)}^0 \frac{dx}{\pi} \frac{\sigma_n \sqrt{1-4\Gamma^2 x^2}}{(x + \sigma_n \tilde{u})^2 (1-4\Gamma^2 x^2) + 1}. \end{aligned} \quad (\text{E14})$$

In the limit of small hybridization and $U \ll 1$, the contribution of the bound states and the influence of the finite

bandwidth can be ignored and we can simplify

$$\begin{aligned} m &\approx \sum_{\sigma_n=\pm 1} \int_{-\infty}^0 \frac{dx}{2\pi} \frac{\sigma_n}{(x + \sigma_n \tilde{u})^2 + 1} \\ &= \frac{1}{\pi} \arctan(Um/\Gamma), \\ Um &\approx \Gamma \tan(\pi m). \end{aligned} \quad (\text{E15})$$

This shows that there is a critical interaction strength above which the magnetic Hartree-Fock solution is energetically favorable over the paramagnetic solution. For $V \rightarrow 0$ we find from eq. (E15) that $U_c^{\text{HF,approx}}(V) = \pi\Gamma = \pi^2 d_0 V^2 = 2\pi V^2$. The numerical value for $V = 0.1$, $U_c^{\text{HF}}(V = 0.1) = 0.06262$ agrees very well with this approximation, $U_c^{\text{HF,approx}}(0.1) = 0.06283$.

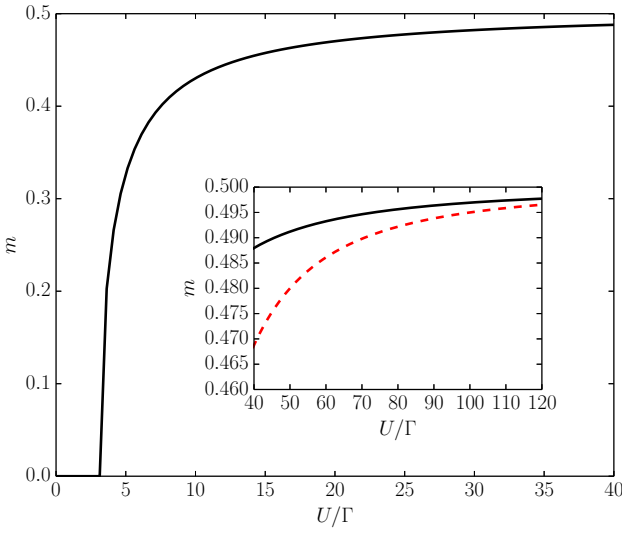


FIG. 15. Magnetization in Hartree-Fock theory as a function of U/Γ for $V = 0.1$ ($\Gamma = 2V^2$ for $d_0 = 2/\pi$). The onset is at $U_c \approx 0.06283 = 3.131\Gamma$. Inset: comparison of the analytic strong-coupling result (E16) (dashed line) with the result of the numerical root for large U/Γ .

Eq. (E15) also shows that $m \rightarrow 1/2$ for $U \gg \Gamma$. However, it incorrectly suggests that $m(U) = 1/2 - 2\Gamma/(\pi U)$ in the large- U limit. Instead, we verified numerically that

$$m(U) \approx \frac{1}{2} - \frac{2V^2}{U^2} + \mathcal{O}(1/U^3). \quad (\text{E16})$$

We show the result for $V = 0.1$ in Fig. 15.

b. Ground-state energy

When we repeat the steps in Sect. C 1, we find

$$\begin{aligned} \Delta E_0^{\text{HF}}(V, U) &= \frac{U}{4} + Um^2 + v_b(V, Um) + v_b(V, -Um) \\ &+ \sum_{\sigma_n=\pm 1} \int_{-1/2}^0 \frac{d\omega}{\pi} \text{Cot}^{-1} \left(\frac{\omega + \sigma_n Um}{\pi \rho_0(\omega) V^2} \right), \end{aligned} \quad (\text{E17})$$

where we took into account the constant term $U/4$ in the definition of $\Delta E_0(U, V)$ and the term Um^2 in eq. (E10). Note that $m \equiv m(U)$ is determined from the solution of the self-consistency equation (E14) for given U .

In the large- U limit, the band contribution is negligible and the pole at $v_b(V, Um) = -Um - V^2/(Um)$ dominates. Together with eq. (E16) we find

$$\Delta E_0^{\text{HF}}(V, U \gg W) = -\frac{2V^2}{U} + \mathcal{O}(V^3/U^2). \quad (\text{E18})$$

This result is readily understood because, in the large- U limit, the host electrons act like a single bath site to which the impurity is coupled. The energy of this two-site model is readily calculated and leads to eq. (E18) in the large- U limit.

c. Host electron polarization

Particle-hole symmetry gives $\langle \hat{c}_{r,\uparrow}^\dagger \hat{c}_{r,\uparrow} + \hat{c}_{r,\downarrow}^\dagger \hat{c}_{r,\downarrow} \rangle = 1$ because $E_{d,\uparrow} = -E_{d,\downarrow}$. However, the Hartree-Fock magnetic moment polarizes the host electrons. In general, the particle numbers are given by

$$N_\sigma = \sum_m \langle \hat{a}_{m,\sigma}^\dagger \hat{a}_{m,\sigma} \rangle = \int_{-\infty}^0 d\omega D_\sigma(\omega), \quad (\text{E19})$$

see Sect. B 2. Using eqs. (A27), (B15), and (B17), we arrive at $(\Delta N_\sigma = N_\sigma - L/2)$

$$\Delta N_\sigma = -\frac{1}{\pi} \int_{-\infty}^0 d\omega \frac{\partial}{\partial \omega} \text{Cot}^{-1} \left(\frac{\omega + E_{d,\sigma} - V^2 \Lambda_0(\omega)}{\pi \rho_0(\omega) V^2} \right). \quad (\text{E20})$$

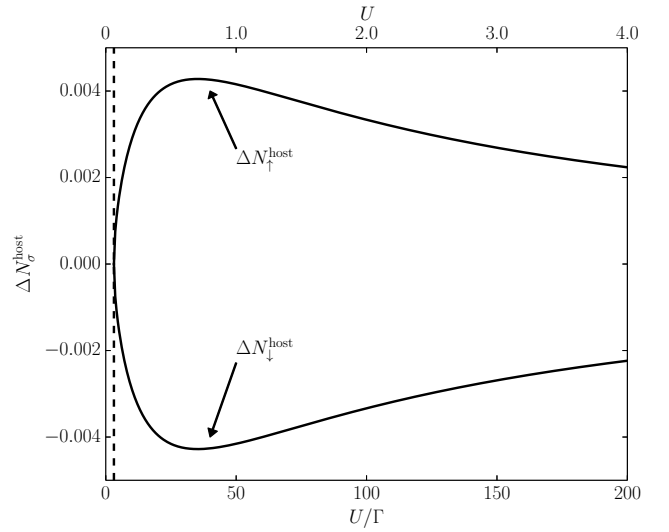


FIG. 16. Host electron particle number $\Delta N_\sigma^{\text{host}} = N_\sigma^{\text{host}} - L/2$, eq. (E22) for $\sigma = \uparrow, \downarrow$ as a function of the magnetization in Hartree-Fock theory for $V = 0.1$.

With $\text{Cot}^{-1}(-\infty) = -\pi$ we find

$$N_\sigma = \frac{L}{2} + 1 - \frac{1}{\pi} \text{Cot}^{-1}(\sigma_n Um / \Gamma) \quad (\text{E21})$$

with $\Gamma = \pi \rho_0(0) V^2 = 2V^2$. By definition, $N_\sigma = N_\sigma^{\text{host}} + n_{d,\sigma}$ with $n_{d,\sigma} = \langle \hat{n}_{d,\sigma} \rangle$ from eq. (E12). Therefore, the host electron particle number is given by

$$N_\sigma^{\text{host}} = \frac{L}{2} + 1 - \frac{1}{\pi} \text{Cot}^{-1}(\sigma_n Um / \Gamma) - n_{d,\sigma}. \quad (\text{E22})$$

For the symmetric Anderson model, $m = 0$ and $n_{d,\sigma} = 1/2$ so that $N_\sigma^{\text{host}} = L/2$ as it should.

The host-electron particle numbers $\Delta N_\sigma = N_\sigma - L/2$ as a function of the magnetization are shown in Fig. 16. It is seen that the impurity barely polarizes the host electrons, even for large magnetization where $n_{d,\uparrow} \approx 1$, $n_{d,\downarrow} \approx 0$. Note that a positive magnetic moment on the impurity also leads to an excess of \uparrow -spins in the host electrons.

d. Spin correlation function

In Hartree-Fock we have $C_{dd}^S = 1/8 + m^2/2$. The result interpolates between the limiting cases $C_{dd}^S(U=0) = 1/8$ for $m=0$ and $C_{dd}^S(U \rightarrow 0) = 1/4$ for $m=1/2$. For the spin correlation between the impurity and the host electrons at site r , Wick's theorem gives

$$C_{dc}^S(r) = \frac{m}{2} \left[\langle \hat{c}_{r,\uparrow}^\dagger \hat{c}_{r,\uparrow} \rangle - \langle \hat{c}_{r,\downarrow}^\dagger \hat{c}_{r,\downarrow} \rangle \right] - \frac{1}{4} \sum_\sigma \left| \langle \hat{d}_\sigma^\dagger \hat{c}_{r,\sigma} \rangle \right|^2. \quad (\text{E23})$$

The first term appears because the Hartree-Fock magnetic moment slightly polarizes the host electrons. Using eq. (A27), the site occupancies are given by

$$\begin{aligned} \langle \hat{c}_{r,\sigma}^\dagger \hat{c}_{r,\sigma} \rangle &= \frac{1}{2} - \frac{V^2}{\pi} \int_{-\infty}^0 d\omega \text{Im} \left[\frac{[Q_r(\omega)]^2}{\omega + \sigma_n Um - \Delta^{\text{ret}}(\omega)} \right] \\ &= \frac{1}{2} + \Delta N_{r,\sigma}^{\text{b}} + \Delta N_{r,\sigma}^{\text{band}}, \\ \Delta N_{r,\sigma}^{\text{b}} &= V^2 Z_{\text{b}}(v_{\text{b}}(V, \sigma_n Um)) [Q_r(v_{\text{b}}(V, \sigma_n Um))]^2, \\ \Delta N_{r,\sigma}^{\text{band}} &= \frac{4V^2}{\pi} \int_{-\pi/2}^0 \frac{(-1)^r A_r(p) dp}{16V^4 + \cos^2 p (\sin p + 2\sigma_n Um)^2} \end{aligned} \quad (\text{E24})$$

with the bound-state weight $Z_{\text{b}}(V)$ and bound-state energy $v_{\text{b}}(V, \sigma_n Um)$ from eq. (B10), $Q_r(\omega)$ from eq. (C14) and

$$A_r(p) = -4V^2 \cos(2pr) + \cos p \sin(2pr) (\sin p + 2\sigma_n Um). \quad (\text{E25})$$

As expected for a bound state, its contribution $\Delta N_{r,\sigma}^{\text{b}}$ decays exponentially for large distances $r \gg 1/(8V^2)$. For $Um \neq 1/2$, the band contribution $\Delta N_{r,\sigma}^{\text{band}}$ contains an exponentially decaying part and a term that decays oscillatory, proportional to $(-1)^r/r$.

The second term in eq. (E23) is evaluated as outlined in Sect. C 3,

$$\begin{aligned} \langle \hat{d}_\sigma^\dagger \hat{c}_{r,\sigma} \rangle &= -\frac{V}{\pi} \int_{-\infty}^0 d\omega \text{Im} \left[\frac{Q_r(\omega)}{\omega + \sigma_n Um - \Delta^{\text{ret}}(\omega)} \right] \\ &= M_{r,\sigma}^{\text{b}} + M_{r,\sigma}^{\text{band}}, \\ M_{r,\sigma}^{\text{b}} &= V Z_{\text{b}}(v_{\text{b}}(V, \sigma_n Um)) Q_r(v_{\text{b}}(V, \sigma_n Um)), \\ M_{2n,\sigma}^{\text{band}} &= \frac{2V}{\pi} \int_{-\pi/2}^0 \frac{(-1)^n \cos p B_{2n}(p) dp}{16V^4 + \cos^2 p (\sin p + 2\sigma_n Um)^2}, \\ B_r(p) &= 4V^2 \sin(rp) + \cos p (\sin p + 2\sigma_n Um) \cos(rp), \\ M_{2n+1,\sigma}^{\text{band}} &= \frac{2V}{\pi} \int_{-\pi/2}^0 \frac{(-1)^{n+1} \cos p C_{2n+1}(p) dp}{16V^4 + \cos^2 p (\sin p + 2\sigma_n Um)^2}, \\ C_r(p) &= -4V^2 \cos(rp) + \cos p (\sin p + 2\sigma_n Um) \sin(rp) \end{aligned} \quad (\text{E26})$$

for $n \geq 0$. For $Um > 1/2$, the matrix elements are small, and the contribution of the second term to the screening are negligible. The results are discussed in the main text.

3. Impurity magnetization from Bethe Ansatz

The Bethe Ansatz results of Ref. [21] employ $H = 2B$ so that the external magnetic field is given by $\mathcal{H} = 2b\Gamma/(g\mu_B)$.

a. Limit of vanishing interactions

Since $b_0(u) \sim \sqrt{u} \rightarrow 0$, we address region II only. We rewrite the magnetic field in the from

$$\Delta b_{II}(p, u) = \sqrt{\frac{1}{8\pi}} \int_0^\infty \frac{d\lambda}{\lambda^{3/2}} \frac{(1 - e^{-2\pi s^2 \lambda})}{\Gamma(\frac{1}{2} + 2u\lambda)} \left(\frac{2u\lambda}{e} \right)^{2u\lambda} \quad (\text{E27})$$

where $\Delta b_{II}(p, u) = b_{II}(p, u) - b_0(u)$ and we set $p = s^2/(2u)$. Taking the limit $u \rightarrow 0$ gives $(\Gamma(1/2) = \sqrt{\pi})$

$$b_{II}(s, 0) = \sqrt{\frac{1}{8\pi^2}} \int_0^\infty \frac{d\lambda}{\lambda^{3/2}} (1 - e^{-2\pi s^2 \lambda}) = s, \quad (\text{E28})$$

i.e., we have $p = b^2/(2u) \rightarrow \infty$ for $u \rightarrow 0$.

The magnetization reads

$$\begin{aligned} m_{II}(s, u) &= \frac{1}{2} - \frac{1}{2} \int_0^\infty \frac{d\lambda}{\sqrt{\pi\lambda}} \frac{e^{-2\pi s^2 \lambda}}{\Gamma(\frac{1}{2} + 2u\lambda)} \left(\frac{2u\lambda}{e} \right)^{2u\lambda} \\ &\quad \times F(2\pi\lambda, u) \end{aligned} \quad (\text{E29})$$

so that we obtain

$$m(b) = \frac{1}{2} - \frac{1}{2} \int_0^\infty \frac{d\lambda}{\sqrt{\pi\lambda}} \frac{e^{-2\pi b^2 \lambda}}{\sqrt{\pi}} F(2\pi\lambda, 0) \quad (\text{E30})$$

in the limit $u \rightarrow 0$. We differentiate $m(b)$ with respect to b^2 and insert the definition of $F(a, 0)$,

$$\begin{aligned} \frac{dm(b)}{db^2} &= \int_{-\infty}^{\infty} \frac{dy}{\pi} \frac{1}{1-y^2} \int_0^{\infty} \frac{d\mu}{2\pi} e^{-(b^2+y^2)\mu} \\ &= \frac{1}{2\pi} \frac{1}{b(1+b^2)}. \end{aligned} \quad (\text{E31})$$

Integrating this expression with respect to b^2 and using $m(0) = 0$ we find

$$m(b) = \frac{1}{\pi} \arctan(b), \quad (\text{E32})$$

as derived for the impurity magnetization of the non-interacting SIAM in the main text.

b. Limit of large magnetic fields

For large b , we again address region II only. Following the lines of the Sect. E 3 a, we can express the magnetic field in the form ($p = s^2/(2u)$)

$$\begin{aligned} b(p, u) &= b_0(u) + s \\ &+ \int_0^{\infty} \frac{d\lambda}{\lambda^{3/2}} \frac{1 - e^{-2\pi s^2 \lambda}}{\sqrt{8\pi}} \left[\frac{(2u\lambda/e)^{2u\lambda}}{\Gamma(\frac{1}{2} + 2u\lambda)} - \frac{1}{\sqrt{\pi}} \right] \\ &= s - \sqrt{2u} Q(\pi s^2/u), \\ Q(y) &= \frac{1}{\sqrt{8\pi}} \int_0^{\infty} \frac{dx}{x^{3/2}} e^{-yx} \left[\frac{(x/e)^x}{\Gamma(\frac{1}{2} + x)} - \frac{1}{\sqrt{\pi}} \right]. \end{aligned} \quad (\text{E33})$$

For the impurity magnetization we find

$$\begin{aligned} m(s, u) &= \frac{1}{\pi} \arctan(s + u/2) + Z(s, u), \\ Z(s, u) &= -\frac{1}{2\sqrt{\pi}} \int_0^{\infty} \frac{d\lambda}{\lambda} e^{-2\pi s^2 \lambda} F(2\pi\lambda, u) \\ &\times \left[\frac{(2u\lambda/e)^{2u\lambda}}{\Gamma(\frac{1}{2} + 2u\lambda)} - \frac{1}{\sqrt{\pi}} \right]. \end{aligned} \quad (\text{E34})$$

These formulae are valid for all magnetic fields in region II. In particular, they include the limit $u \rightarrow 0$.

For large fields, we see from (E33) that $s \approx b \gg 1$ and that only small x contribute to the integrand of $Q(y)$ for $y = \pi s^2/u \gg 1$. Using the small- x expansion for the integrand leads to⁴⁰

$$Q(y \gg 1) \approx -\frac{1 + \ln(y)}{\sqrt{8\pi y}}. \quad (\text{E35})$$

We use $s \approx b$ in this term to find

$$s = b - \frac{u}{2\pi b} [1 + \ln(\pi b^2/u)] \quad (\text{E36})$$

for $b^2 \gg u/\pi$ from eq. (E33). The same line of arguments gives

$$Z(s, u) \approx -\frac{u}{\pi^2} \left(\frac{1 - \ln(\pi s^2/u)}{2s^3} \right), \quad (\text{E37})$$

where we used $F(a \rightarrow 0, u) \approx 2\sqrt{a/\pi}$. We replace s by b for large fields, insert this result into eq. (E34), and find

$$m_{II}(b \gg \sqrt{u/\pi}) \approx \frac{1}{2} - \frac{1}{\pi b} + \frac{u}{2\pi b^2} + \frac{4\pi - 12u - 3\pi u^2}{12\pi^2 b^3} \quad (\text{E38})$$

up to and including third order in $1/b$. There are no logarithmic corrections to this order.

In fact, there are no logarithmic terms to all orders of the $1/b$ expansion because, for $b \gg 1$, both $b(p, u)$ and $m_{II}(p, u)$ can be expressed in terms of a series with odd powers in the parameter $1/\sqrt{z}$ where z obeys $p = z - \ln(2\pi e z)/(2\pi)$.²¹ Therefore, at large values of the external field, the impurity magnetization does not show any signs of the logarithmic Doniach-Šunjić-Hamann tails in the impurity spectral function.^{10–12,37}

* florian.gebhard@physik.uni-marburg.de

¹ P. W. Anderson, Phys. Rev. **124**, 41 (1961)

² P. W. Anderson, Rev. Mod. Phys. **50**, 191 (1978)

³ A. C. Hewson, *The Kondo Problem to Heavy Fermions* (Cambridge University Press, Cambridge, 1993)

⁴ S. G. Jakobs, M. Pletyukhov, and H. Schoeller, Phys. Rev. B **81**, 195109 (2010)

⁵ M. Kinza, J. Ortloff, J. Bauer, and C. Honerkamp, Phys. Rev. B **87**, 035111 (2013)

⁶ J. F. Rentrop, V. Meden, and S. G. Jakobs, Phys. Rev. B **93**, 195160 (2016)

⁷ C. Zener, Phys. Rev. **81**, 440 (1951)

⁸ J. Kondo, Progress of Theoretical Physics **32**, 37 (1964)

⁹ R. Bulla, T. Costi, and T. Pruschke, Rev. Mod. Phys. **80**, 395 (2008)

¹⁰ D. E. Logan, M. P. Eastwood, and M. A. Tusch, Journal

of Physics: Condensed Matter **10**, 2673 (1998)

¹¹ D. E. Logan and M. T. Glossop, Journal of Physics: Condensed Matter **12**, 985 (2000)

¹² M. R. Galpin, A. B. Gilbert, and D. E. Logan, Journal of Physics: Condensed Matter **21**, 375602 (2009)

¹³ L. Borda, Phys. Rev. B **75**, 041307 (2007)

¹⁴ A. K. Mitchell, M. Becker, and R. Bulla, Phys. Rev. B **84**, 115120 (2011)

¹⁵ B. Lechtenberg and F. B. Anders, Phys. Rev. B **90**, 045117 (2014)

¹⁶ S. Florens and I. Snyman, Phys. Rev. B **92**, 195106 (2015)

¹⁷ S. Ghosh, P. Ribeiro, and M. Haque, Journal of Statistical Mechanics: Theory and Experiment **2014**, P04011 (2014)

¹⁸ A. Holzner, I. P. McCulloch, U. Schollwöck, J. von Delft, and F. Heidrich-Meisner, Phys. Rev. B **80**, 205114 (2009)

¹⁹ N. Andrei, Phys. Rev. Lett. **45** (1980)

²⁰ P. B. Wiegmann, *Journal of Physics C: Solid State Physics* **14**, 1463 (1981)

²¹ P. B. Wiegmann and A. M. Tsvelick, *Journal of Physics C: Solid State Physics* **16**, 2281 (1983)

²² A. M. Tsvelick and P. B. Wiegmann, *Journal of Physics C: Solid State Physics* **16**, 2321 (1983)

²³ K. Schönhammer, *Phys. Rev. B* **42**, 2591 (1990)

²⁴ F. Gebhard, *Phys. Rev. B* **41**, 9452 (1990)

²⁵ See Supplemental Material at [URL will be inserted by publisher] for the derivation of the results for the non-interacting SIAM (resonant level model) and the Hartree-Fock theory.

²⁶ O. Legeza, F. Gebhard, and J. Rissler, *Phys. Rev. B* **74**, 195112 (2006)

²⁷ A. E. Feiguin and C. A. Büsser, *Phys. Rev. B* **84**, 115403 (2011)

²⁸ J. R. Schrieffer and P. A. Wolff, *Phys. Rev.* **149**, 491 (1966)

²⁹ Z. M. M. Mahmoud and F. Gebhard, *Ann. Phys. (Berlin)* **527**, 794 (2015)

³⁰ N. Kawakami and A. Okiji, *Physics Letters A* **86**, 483 (1981)

³¹ S. R. White, *Phys. Rev. Lett.* **69**, 2863 (1992)

³² S. R. White, *Phys. Rev. B* **48**, 10345 (1993)

³³ O. Legeza, J. Röder, and B. A. Hess, *Phys. Rev. B* **67**, 125114 (2003)

³⁴ O. Legeza and J. Sólyom, *Phys. Rev. B* **70**, 205118 (2004)

³⁵ K. Yamada, *Progress of Theoretical Physics* **53**, 970 (1975)

³⁶ We correct a typo in the expression in Ref. [21] by replacing $\pi^{1/2}$ by $\pi^{3/2}$.

³⁷ S. Doniach and M. Šunjić, *Journal of Physics C: Solid State Physics* **3**, 285 (1970)

³⁸ A. Okiji and N. Kawakami, *Solid State Communications* **43**, 365 (1982)

³⁹ T. Linneweber, J. Büinemann, Z. M. M. Mahmoud, and F. Gebhard, *Journal of Physics: Condensed Matter* **29**, 445603 (2017)

⁴⁰ *Mathematica, Version 10* (Wolfram Research, Inc., Champaign, 2015)

⁴¹ J. Goldstone, *Proceedings of the Royal Society of London A: Mathematical, Physical and Engineering Sciences* **239**, 267 (1957)

⁴² D. Ruhl and F. Gebhard, *Journal of Statistical Mechanics: Theory and Experiment* **2006**, P03015 (2006)